Journal of Hydrology 673 (2026) 135413

Contents lists available at ScienceDirect

Journal of Hydrology

journal homepage: www.elsevier.com/locate/jhydrol

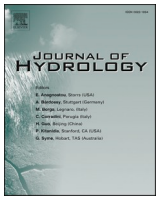

Research papers

A new comprehensive monitoring framework for global drought assessment

Alhassane Bah [a,b,c], Asim Biswas [d], Hao Feng [e], Qiang Yu [e], Qianfeng Wang [f], Yi Li [a,b,c,*]

[a] College of Water Resources and Architecture Engineering, Key Lab of Agricultural Water and Soil Engineering of Education Ministry, Northwest A&F University, Yangling 712100, China
[b] Academy of Plateau Science and Sustainability, Qinghai Normal University, Xining 810008, China
[c] Northwest A&F University Shenzhen Research Institute, Shenzhen 518000, China
[d] School of Environmental Sciences, University of Guelph, Guelph, Ontario N1G 2W1, Canada
[e] College of Soil and Water Conservation Science and Engineering, Northwest A&F University, Yangling 712100, China
[f] College of Environment & Safety Engineering, Fuzhou University, Fuzhou 350116, China

ARTICLE INFO

This manuscript was handled by Ashok Mishra

Keywords:
Drought monitoring
Principal Component Analysis (PCA)
Climate change
Multidimensional drought assessment
Composite drought index

ABSTRACT

We present a novel Comprehensive Drought Index (CoDI) for global drought assessment that integrates meteorological, agricultural, and hydrological drought dimensions. Using Principal Component Analysis (PCA), CoDI optimally combines the Standardized Precipitation Index (SPI), Standardized Soil Moisture Index (SSI), and Standardized Runoff Index (SRI) with continent-specific probability distributions.

We validated CoDI across sixty (60) major basins spanning multiple continents and against 22 historical drought events. The CoDI demonstrates substantial agreement with other indices in capturing historical and seasonal drought events, including scPDSI and SPEI. The Terrestrial Water Storage Anomaly (TWSa) response to CoDI exhibits short lag time (0 to 2 months) in the majority of the 60 selected basins, in contrast to the scPDSI, which displays longer lag times. The CoDI was able to capture the seasonal drought events in the Australia's southwestern region that occurred from January to March 2011 while the SPEI_cru captured only the January drought event. This demonstrate the capability of CoDI to capture different types of drought conditions compare to the SPEI and the importance of integrating meteorological, hydrological, and agricultural drought components.

Global drought characterization from 1982 to 2018 identified key drought hotspots in the Sahel, Central Asia, and parts of South America, with drought duration ranging from 40-131 months. CoDI provides consistent drought characterization across diverse hydroclimatic regimes at multiple timescales, enabling improved early warning, water resource management, and climate adaptation strategies. This framework represents a significant advancement in transforming drought monitoring from single-variable approaches to integrated, multidimensional assessment.

1. Introduction

Droughts represent one of the most complex and destructive natural disasters, affecting ecosystems, water resources, agriculture, and human societies worldwide (Cai et al., 2023; Yang et al., 2018). Unlike other sudden-onset extreme events, droughts develop gradually, pervade vast geographical areas, and can persist for months to years, making them particularly challenging to monitor, characterize, and mitigate (Dilanka Athukoralalage et al., 2021; Fabian et al., 2023; Niu et al., 2024). As global climate change accelerates, drought conditions are projected to intensify in many regions through increased temperatures, enhanced atmospheric moisture demand, and altered precipitation patterns (Balint et al., 2013; Herweijer and Seager, 2008; Jiefeng et al., 2018).

Moreover, the economic impact of droughts is staggering, with annual global losses estimated between $6–8 billion, significantly exceeding costs from other natural disasters (Yang et al., 2018). These impacts extend beyond immediate economic damage to affect long-term ecosystem functioning, with recent severe drought events triggering significant vegetation degradation, agricultural failures, and cascading hazards including wildfires and heat waves (Chiang et al., 2021; Ismail et al., 2024; Xu et al., 2023; Zhang et al., 2019; Zhang et al., 2021). The Global Precipitation Climatology Center has documented alarming

* Corresponding author at: College of Water Resources and Architecture Engineering, Key Lab of Agricultural Water and Soil Engineering of Education Ministry, Northwest A&F University, Yangling 712100, China.
E-mail address: liyi@nwafu.edu.cn (Y. Li).

https://doi.org/10.1016/j.jhydrol.2026.135413
Received 11 December 2025; Received in revised form 20 March 2026; Accepted 25 March 2026
Available online 28 March 2026

trends of increasing drought duration, severity, and frequency across multiple vulnerable regions, including the Amazon, East Asia, West Africa, Central America, and the Mediterranean (Niu et al., 2024). Climate projections suggest these trends will worsen, expanding to additional regions across the Americas, Asia, Europe, and Africa.

The multidimensional nature of drought manifesting simultaneously as meteorological, agricultural, and hydrological phenomena necessitates comprehensive monitoring approaches that can capture its complexity (Han et al., 2022; Pendergrass et al., 2020). Traditional drought indices have focused on singular aspects of drought (e.g., rainfall deficits, soil moisture anomalies, or streamflow reductions), but these approaches fail to capture the interconnected cascade of drought processes across the hydrological cycle (Hao et al., 2016; J. Yang et al., 2018). While recent years have seen the development of several composite drought indices (Table 1), these efforts remain predominantly focused on regional applications with limited global transferability (Han et al., 2022; Jiaoa et al., 2019).

A critical research gap exists in developing a truly global, comprehensive drought monitoring framework that integrates meteorological, agricultural, and hydrological dimensions of drought across diverse climate regimes. This gap is particularly acute given the accelerating climate change impacts on water resources and the pressing need for early warning systems that can support adaptive management strategies. Current global drought monitoring systems face several key limitations:

(1) Insufficient integration of meteorological, hydrological, and agricultural drought components at global scale into a unified framework,
(2) Limited validation across diverse hydroclimatic regions at global scale

To address these limitations, we introduce a novel Comprehensive Drought Index (CoDI) designed specifically for global-scale drought assessment and monitoring. Unlike previous composite indices that have been developed for specific regions or climate types, CoDI represents a methodological advance in global drought characterization by:

1. Synthesizing three fundamental drought indices the Standardized Precipitation Index (SPI), Standardized Soil Moisture Index (SSI), and Standardized Runoff Index (SRI) to capture the multidimensional nature of drought at the global scale
2. Employing Principal Component Analysis to optimally weight and combine these indices, preserving maximum information content while reducing redundancy
3. Implementing a flexible framework that can function across diverse hydroclimatic regimes and data availability scenarios
4. Validating performance across 60 major river basins spanning multiple continents and climate zones, along with documented historical drought events at local, regional, and continental scales
5. Characterizing global drought patterns through comprehensive assessment of drought duration, severity, and frequency from 1982 to 2018

This research contributes to transforming drought management from reactive to proactive approaches by providing a robust methodological framework for early detection, consistent characterization, and improved understanding of drought dynamics across the earth system. By integrating meteorological, agricultural, and hydrological drought perspectives, CoDI offers a more holistic representation of drought conditions than previously possible, with critical applications for water resource management, agricultural planning, disaster risk reduction, and climate adaptation strategies.

2. Materials and methods

2.1. Study area

Our study focused on global drought assessment with spatial coverage spanning 60°S-90°N and 180°W-180°E. To validate the proposed CoDI at local scale and evaluate its performance across diverse hydroclimatic zones and different continents, we selected the top 60 major river basins in terms of area size (see Fig. 1 and Table 2). This study employed the climate zone classification established by Beck et al, (2018). This classification defines five (5) climate zones: The Tropical

Table 1
Summary of composite drought indices focusing on regional or watershed study areas presented in the last decade.

Name	Variables	Dataset	Indices	Study area	Approach	Reference
PMDI	Precipitation, Air Temperature, Wind Speed, Air Pressure, Relative Humidity, and Sunshine	GIMMS3g, MODIS, TRMM, AMSR-E, and GLEAM	VCI, TCI, PCI, and SMCI	Central China, (Loess Plateau (LP) and Qinling Mountains (QL))	PCA-RF	Zhang et al., (2021)
MCDIs	Precipitation, Soil moisture, NDVI, and LST	MODIS,, GLDAS-2.1, TRMM	TCI, VCI, PCI, and SMCI	North China, Shandong Province	Multivariable linear regression	Liu et al., (2020)
SDI	Precipitation, Temperature,, NDVI and LST	MODIS and TRMM, and AVHRR	PCI, TCI, and VCI	Shandong province, China	PCA	(Du et al., 2013)
MMSDI	Precipitation, Soil moisture, and Solar-Induced chlorophyll Fluorescence	IMD, Global GOSIF_v2, ESA CCI, and SM_v6.1	SPI, SSI, and SSIFI	Indo-Gangetic Plains (IGP) in India	Nonparametric empirical joint distribution	(Kumar & Chu, 2024)
MSDI	Precipitations and soil moisture	Climate Prediction Center (CPC)	SPI and SSI	California and North Carolina	Copulas	(Hao & AghaKouchak, 2013)
CCDIs	Precipitation, Evaporation,, Runoff, Salinity, NDVI and LST	MODIS, Fujian Provincial Department of Ecology and Environment official website	PNL, PEN, PEL, PRN, NDVI, SNL, RSN, RSL, and PER	coastal areas of southeastern China: Jinjiang River Basin (JJRB) and the Jiulong River Basin (JLRB)	Entropy-weighted Euclidean distance method	(Xu et al., 2023)
SPERSI	rainfall, temperature, runoff and soil moisture	GLDAS	SPEI, SRI and SSMI	Yellow River basin, China	Copulas	Wang et al., (2024)
PMDI	Soil moisture and Runoff	PRISM, NCEP, CFSR, AND MOPEX	….	Texas (USA)	Copulas	(Zhang et al., 2019)
MDI	Precipitation, Runoff, Evapotranspiration and Soil moisture	NOAA Cooperative Observer (Coop) stations, PRISM, and Variable Infiltration Capacity (VIC) model	SPEI, SRI, and SMI	Texas	KernelEntropy Component Analysis (KECA)	(Rajsekhar et al., 2015)

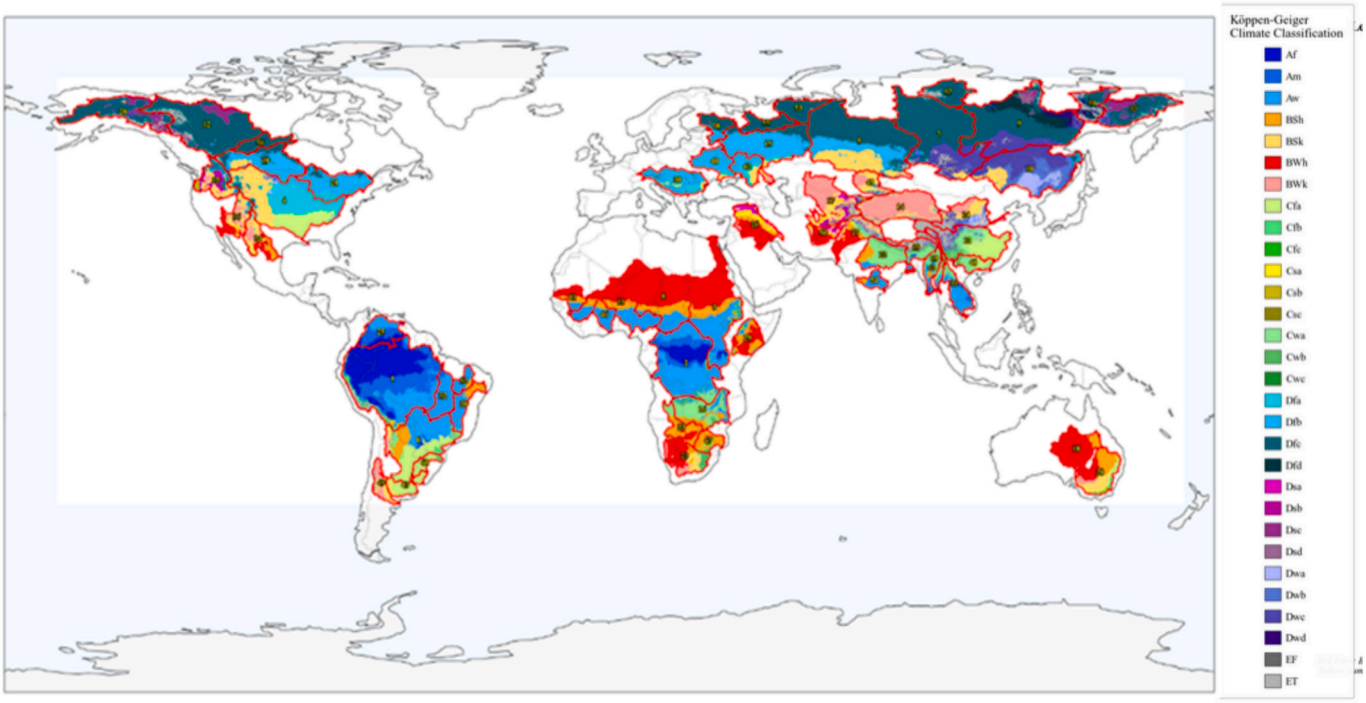

Fig. 1. Climate zones of the 60 selected river basins for CoDI validation. This climate zone classification is based on Beck et al, (2018) classification. Look at the map and identify the ID number of each basin, then consult Table 2 for further information regarding each basin, including name. ID, and area size.

Table 2
Summary of the 60 basins with their rank (ID) and area size.

ID	RIVERBASIN	Area (Km^2)	ID	RIVERBASIN	Area (Km^2)
1	AMAZON	5979268.055	31	MEKONG	785555.5741
2	CONGO	3713531.14	32	TOCANTINS	774199.1827
3	NILE	3360720.785	33	OKAVANGO	693775.1016
4	MISSISSIPPI	3247884.396	34	RIO GRANDE	675371.7244
5	OB	3047423.161	35	COLUMBIA	670902.2111
6	PARANA	2652237.519	36	COLORADO	662594.4535
7	YENISEY	2511287.015	37	KOLYMA	654424.0821
8	CHAD	2476583.837	38	SAO FRANCISCO	638631.1196
9	LENA	2459150.505	39	BRAHMAPUTRA	541994.8325
10	AMUR	2243993.761	40	DNIEPER	510962.2279
11	NIGER	2127756.777	41	SENEGAL	459054.3862
12	MACKENZIE	1799653.672	42	DON	438659.1444
13	YANGTZE	1752042.098	43	RIO DE LA PLATA	428265.4019
14	TARIM HE	1566705.542	44	IRRAWADDY	423864.1018
15	VOLGA	1427629.922	45	LAKE BALKHASH	415690.1425
16	ZAMBEZI	1381193.923	46	VOLTA	413573.5738
17	ARAL SEA	1375596.73	47	LIMPOPO	413506.5054
18	LAKE EYRE	1217349.533	48	ZHU	412852.7668
19	NELSON	1108998.331	49	COLORADO	401790.5582
20	MURRAY	1057783.098	50	HAMUN	401541.962
21	SAINT LAWRENCE	1055658.106	51	INDIGIRKA	342001.8319
22	GANGES	1008816.292	52	PARNAIBA	333724.9283
23	ORANGE	979515.8143	53	PECHORA	314926.9767
24	YELLOW RIVER	965147.0026	54	GODAVARI	311073.2474
25	ORINOCO	943528.1002	55	SEVERNAYA DVINA	307537.9739
26	SHATT AL ARAB	937668.1498	56	CHURCHILL	303174.7224
27	INDUS	866954.4188	57	KHATANGA	301503.118
28	YUKON	834687.0128	58	NEVA	281756.2753
29	JUBBA	799670.7525	59	SALWEEN	266889.6187
30	DANUBE	797102.0775	60	URUGUAY	266730.1568

climates (Group A) are characterized by consistence warm and varying precipitation. This type includes Af, Am, and Aw. The Dry climates (Group B) includes BWh, BSk, BSh, and BWk. Temperate climates (Group C) are defined by mild-latitude and distinct seasonal precipitation. This type includes Cwa, Cwb, Csc, etc… The Continental climates (Group D) are characterized by severe winters and high temperature. This type includes Dsa, Dsb, Dsc, etc…and the Polar climates (Group E) are dominated by the tundra. This category includes ET and EF.

2.2. Data sources and processing

We utilized multiple global gridded datasets to construct and validate the CoDI framework:

2.2.1. Precipitation data

Monthly gridded precipitation data (0.5°×0.5° resolution) were obtained from the Climate Research Unit Gridded Time Series (CRU TS) dataset covering 1982–2018. This dataset provides high-resolution global land-based precipitation measurements derived from meteorological station networks (Ian et al., 2020).

2.2.2. Runoff data

Global monthly gridded runoff data (0.5°×0.5° resolution) covering 1982–2018 were acquired from the GRUN global runoff reconstruction dataset (https://figshare.com/articles/dataset/G-RUN_ENSEMBLE/12794075). This dataset was generated using a machine learning approach that predicts runoff from temperature and precipitation reanalysis data (Ghiggi et al., 2019).

2.2.3. Soil moisture data

Global soil moisture data were obtained from the FLDAS Noah surface model L4 provided by NASA's GES DISC. This dataset combines Modern-Era Research and Applied Retrospective Analysis (MERRA-2) with Climate Hazards Panel Infrared Precipitation Stations (CHIRPS) rainfall data, downscaled using NASA's Terrestrial Data Toolkit. The data were originally at 0.1°×0.1° resolution and resampled to 0.5°×0.5°

using bilinear interpolation to match other datasets. The temporal coverage spans from January 1982 to December 2018 at monthly intervals.

2.2.4. Standardized precipitation evapotranspiration index (SPEI_cru)

For validation purposes, we utilized the global SPEI (SPEI_cru) database (https://spei.csic.es/) at 0.5°×0.5° spatial resolution from 1982 to 2018. This dataset, based on CRU monthly potential evapotranspiration and precipitation data, provides multi-scale drought information (1–48 months) and has been extensively validated in previous studies.

2.2.5. ERA5 based indices

For validation purposes, we also utilize SPEI (SPEI_era5) and SPI (SPI_era5) based ERA5 data. These drought indices datasets came from the fifth generation ECMWF reanalysis system (ERA5), which provides both probabilistic and deterministic long-term global climate monitoring (Keune et al., 2025). Two well-known drought indices are included in this global dataset, which is publicly available via a data store hosted by the ECMWF: the Standardized Precipitation Index (SPI) and the Standardized Precipitation Evapotranspiration Index (SPEI). For the complete ERA5 climatology from 1940 to the present, both indices are provided and are computed across accumulation periods ranging from one month to four years.

The ERA5-Drought dataset is available through the ECMWF-hosted Cross Data Store (XDS) via https://doi.org/10.24381/9bea5e16.

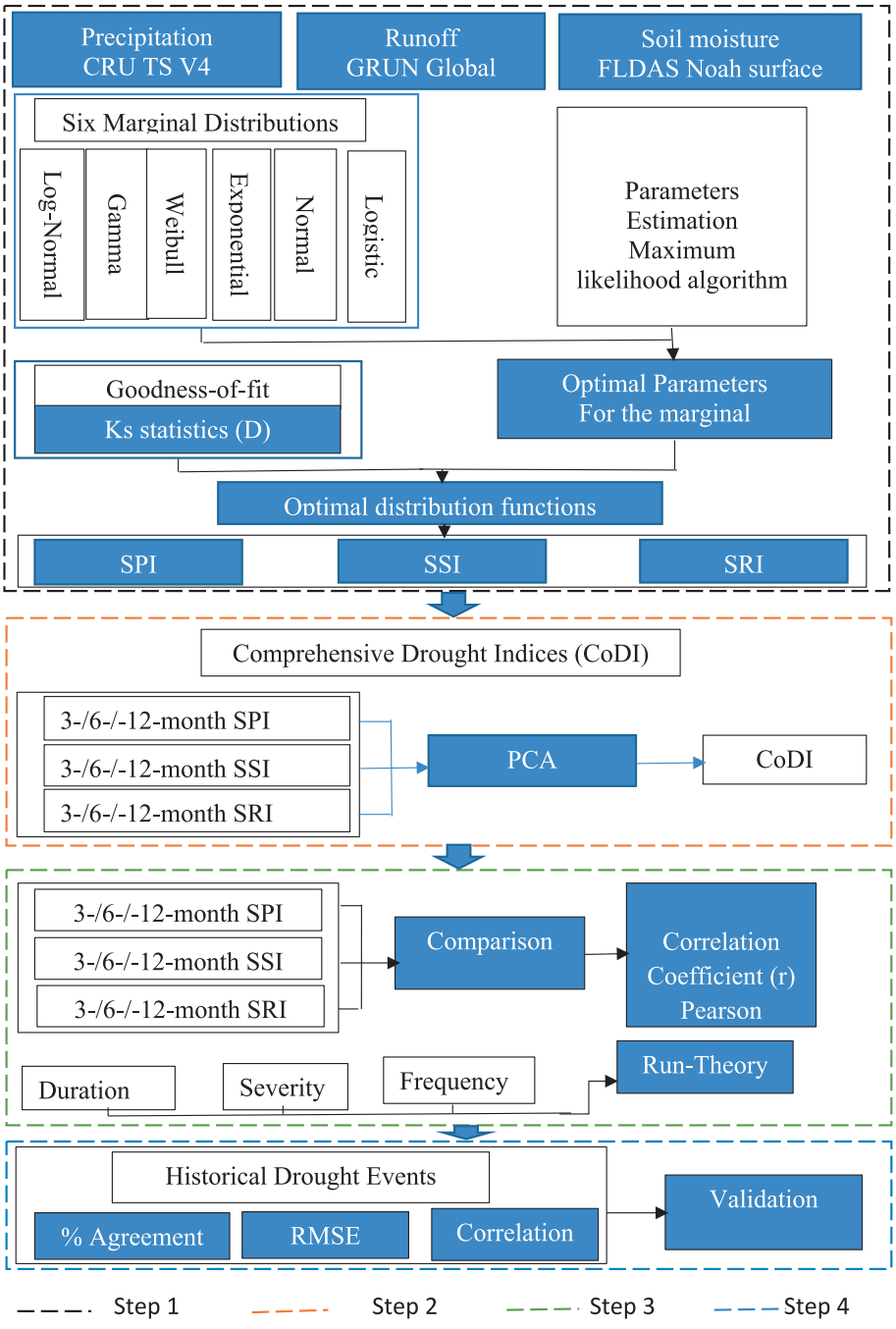

Fig. 2. Framework for the CoDI construction and validation.

2.2.6. Self-calibrated palmer drought severity index (scPDSI)

For validation purposes, we also utilize scPDSI. Wells et al., (2004) introduced the scPDSI metric and provide comprehensive details on how to calculate it. Palmer's (1965) original PDSI was modified to create the scPDSI, which aims to improve comparability of results from various climate regimes. Similar to the PDSI, the scPDSI is computed using temperature and precipitation time series together with fixed parameters related to the surface and soil properties at each location (Van Der Schrier et al., 2013). The data can be downloaded from https://crudata.uea.ac.uk/cru/data/drought/.

2.2.7. Reconstructed terrestrial water storage anomalies (TWSa)

For validation purpose, we used the GRAiCE monthly TWSa reconstructions from 1984 to 2018 at 0.5° spatial resolution. Four climate-driven models that reconstruct TWSA time series prior to the GRACE era (i.e., before 2002) and replicate GRACE/GRACE-FO TWSA observations. We selected the TWSa to further validate the CoDI for its ability to reflect water scarcity from surface to subsurface, which align with the new index's comprehensive integration of meteorological, hydrological, and agricultural drought dimensions. Additional details regarding GRAiCE datasets are available from (Palazzoli et al., 2025). We used the GRAiCE_BiLSTMnoLC product among the GRAiCE's four products. This product is a variant of BiLSTM model excluding Land Cover and Solar-Induced Fluorescence (SIF) data.

All datasets were harmonized to a consistent 0.5°×0.5° spatial resolution and temporal coverage of 1982–2018 at monthly intervals. Data quality control procedures were applied to ensure consistency and reliability across the global domain.

2.3. Methodological framework for CoDI construction

The development of CoDI followed a systematic four-step approach (Fig. 2):

Step 1: Selection of optimal probability distributions for drought index calculation
Step 2: Computation of univariate drought indices (SPI, SRI, and SSI)
Step 3: Integration of indices using Principal Component Analysis
Step 4: Validation of CoDI through comparison with historical drought events

2.3.1. Determination of optimal probability distributions

A critical step in constructing reliable drought indices is selecting appropriate probability distributions that best characterize the statistical behavior of hydroclimatic variables across different regions. We evaluated six candidate distribution functions (Table 3) for fitting monthly runoff and soil moisture time series: Log-Normal, Gamma, Weibull, Exponential, Normal, and Logistic.

For precipitation data, we adopted the widely accepted Gamma distribution following established practice in SPI calculation (Stagge et al., 2015). For runoff and soil moisture, we identified the optimal distributions by continent using the Kolmogorov-Smirnov (KS) goodness-of-fit test. The KS statistic (D) measures the maximum vertical difference between the theoretical cumulative distribution function and the empirical distribution function:

$$D = max\left(m_i\left|CDF(x_i) - \frac{r-1}{n}, \frac{r}{n} - CDF(x_i)\right|\right) \quad (1)$$

Where r is the rank of the i^{th} observation in ascending order. The distribution with the smallest D value was selected as optimal for each variable and continent.

2.3.2. Computation of univariate drought indices

Using the identified optimal distributions, we calculated three standardized drought indices:

2.3.2.1. Standardized precipitation index (SPI). Characterizes meteorological drought based on precipitation anomalies. SPI is widely used due to its versatility because it can be computed across several timescales. This enables the monitoring of both short-term agricultural effects such as soil moisture and long-term hydrological impacts such as reservoir levels (Mishra & Singh, 2010). However, univariate indices have certain limitations. For instance, Mishra & Singh, (2010) highlighted that the varying length of precipitation record might modify the fitted probability distribution and result in inconsistent SPI values. Particular challenges emerges for long-term timescales (exceeding 24-month), where the fitting of distribution may be biased in sparse data regions (Mishra & Singh, 2010). In addition, the exclusion of variables such as temperature, PET, wind speed, and soil moisture constitute a major limitation for generating reliable drought information under a warming climate (Mukherjee et al., 2018; Sabut & Mishra, 2026).

2.3.2.2. Standardized runoff index (SRI). Represents hydrological drought through runoff anomalies. SRI effectively complements SPI in distinguishing hydrological aspects of drought (Mishra & Singh, 2010). Similar to the SPI, accurate SRI computation requires long-term and high quality runoff data. In regions with spares data, the index may be less reliable. In addition, the choice of probability distribution can significantly affect the results.

2.3.2.3. Standardized soil moisture index (SSI). Captures agricultural drought via soil moisture anomalies. The application of in situ soil moisture conditions as a drought indicator has been constrained mainly by the limitation of the record (i.e., less than 20 years for most stations), complicating the standardization and assessment of the severity (i.e., 2nd vs. 20th percentile) or rarity of soil moisture conditions (Leeper et al., 2021). Therefore, in this study we used the FLDAS Noah surface model L4 provided by NASA's GES DISC, Which facilitate the

Table 3
The 6 distribution functions and their probability density functions (PDF) used in this study.

Distributions	Parameter 1 and 2	Functions (F(x))
Log-Normal	Mean: u Variance:σ^2	$f(x) = \frac{1}{x\sigma\sqrt{2\pi}} e^{-\frac{(lnx-u)^2}{2\sigma^2}}$
Gamma	Shape: α Scale: β	$f(x,\beta,\alpha) = \frac{\beta^{\alpha}}{\Gamma_{(\alpha)}} x^{\alpha-1} e^{-\beta x}$
Weibull	Shape: α Scale: β	$f(x) = \frac{\alpha}{\beta}\left(\frac{x}{\beta}\right)^{\alpha-1} e^{-(x/\beta)^{\alpha}}$
Exponential	Rate: λ	$f(x) = \lambda e^{-\lambda x}$
Normal	Mean: u Variance:σ^2	$f(x) = \frac{1}{\sqrt{2\pi}\sigma} e^{-\frac{(x-u)^2}{2\sigma^2}}$
Logistic	Location: μ Scale: s	$f(x) = \frac{e^{-(x-\mu)/s}}{s(1+e^{-(x-\mu)/s})^2}$

development of long-term soil moisture time series using historical simulations. The extensive time series enable the standardization of predicted soil moisture observations for use in drought monitoring applications (Leeper et al., 2021).

The cumulative distribution function F(x) for each variable was transformed to the standard normal distribution using:

$$SPI\,/\,SRI\,/\,SSI = \begin{cases} -\left(t - \dfrac{c_0 + c_1 t + c_2 t^2}{1 + d_1 t + d_2 t^2 + d_3 t^3}\right), if 0 < p \le 0.5 t = \sqrt{\ln \dfrac{1}{p^2}} (a) \\ +\left(t - \dfrac{c_0 + c_1 t + c_2 t^2}{1 + d_1 t + d_2 t^2 + d_3 t^3}\right), if 0.5 < p \le 1 t = \sqrt{\ln \dfrac{1}{(1-p^2)}} (b) \end{cases} \quad (2)$$

Where p = 1-F(x), and the coefficients are d_1=1.432788, d_2=0.189269, d_3=0.001308, c_0=2.515517, c_1=0.802853, and c_2=0.010328.

We calculated these indices at three key timescales (3, 6, and 12-month) to capture drought dynamics at different temporal resolutions. Shorter timescales (3-month) primarily reflect meteorological drought conditions, intermediate scales (6-month) capture agricultural impacts, and longer timescales (12-month) represent hydrological drought effects on water resources.

2.3.3. Integration through principal component analysis

To create CoDI, we employed Principal Component Analysis (PCA), a multivariate statistical technique that identifies relationships between variables and expresses their relative importance in an organized manner (Johnny Jesudhas et al., 2024; Liu et al., 2019). For each grid cell globally, we applied PCA to the three standardized indices (SPI, SRI, and SSI) to extract the principal components that explain the maximum variance in the original data.

The first two principal components (PC_1 and PC_2) typically accounted for over 85% of the total variance across the three drought indices. We computed CoDI as a weighted combination of these two components:

$$v_1 = \frac{\tau_1}{(\tau_1 + \tau_2 + \tau_3)} \quad (3)$$

$$v_2 = \frac{\tau_2}{(\tau_1 + \tau_2 + \tau_3)} \quad (4)$$

$$CoDI = (v_1 * PC_1) + (v_2 * PC_2) \quad (5)$$

Where v_1 and v_2 are the normalized variances, τ_1, τ_2, and τ_3 are the eigenvalues from the PCA, and PC_1 and PC_2 are the first and second principal components. This approach ensures that the most influential drought dimensions receive appropriate weighting in the final index.

The resulting CoDI values follow the same classification scheme as the individual standardized indices, with negative values indicating drought conditions of increasing severity (Table 4).

2.3.4. Drought characterization using run theory

We applied run theory to characterize drought events and extract key drought parameters from the CoDI time series. Run theory defines drought events as periods when an index remains continuously below a specified threshold (Wu et al., 2021). We established a threshold of zero for CoDI, with negative values indicating drought conditions of varying severity.

For each grid cell globally, we extracted three fundamental drought characteristics (Fig. 3):

Drought Duration: The number of consecutive months with CoDI values below the threshold.

Drought Severity: The cumulative deficit (sum of CoDI values) during a drought event.

Drought Frequency: The number of drought events over the study period (1982–2018).

Table 4
Drought indices classification applied in this study.

Drought Categories	Indices values
No Drought (ND)	Higher than 0
Mild Drought (MiD)	0 < Index ≤ -0.5
Moderate Drought (MD)	−0.5 ≤ Index ≤ -1.0
Severe Drought (SD)	−1.0 ≤ Index ≤ -1.5
Extreme Drought (ED)	Less than −1.5

2.3.5. Validation framework

We implemented a comprehensive validation strategy to assess CoDI performance across spatial scales and drought types:

1. **Global and Basin-scale Correlation Analysis**: We calculated correlation coefficients between CoDI and established drought indices (SPI, SRI, SSI, scPDSI, TWSa, SPEI_era5, and SPEI_cru) at multiple timescales (3, 6, and 12-month) globally and for the sixty (60) selected river basins.
2. **Seasonal Performance Evaluation**: We examined correlations between CoDI and other indices across different seasons to assess temporal consistency.
3. **Drought Area Detection Comparison**: We compared the percentage of drought-affected areas detected by CoDI, scPDSI, SPEI_era5, and SPEI_cru across different drought severity classes for the 60 river basins.
4. **Terrestrial Water Storage response to drought indices**: We compared the response of TWSa to CoDI, scPDSI, and both variant of SPEI at 12-month timescale in the 60 selected basins by calculating the lag time.
5. **Historical Drought Event Validation**: We evaluated CoDI performance in capturing eight well-documented historical drought events in the Limpopo and Volta River Basins (Table 5), computing percentage agreement, root mean square error (RMSE), and correlation coefficient with established indices. In addition, we evaluated the response of TWSa to CoDI, scPDSI, and both variant of SPEI by calculating the correlation between TWSa and these indices.
6. **Continental and Regional Validation**: We assessed CoDI performance across 14 historical drought events in various regions and continents, including Niger, Australia, China, Eastern Europe, Southwestern Russia, Kazakhstan, and the Sahel, comparing against SPEI_cru, SPEI_era5, scPDSI, and SPI_era5 using percentage agreement, RMSE, and correlation metrics. The 14 drought events were selected from the *EM-DAT database* (https://public.emdat.be/data).

This validation approach ensures robust assessment of CoDI across diverse spatial domains, temporal scales, and drought characteristics, providing a comprehensive evaluation of its utility for global drought monitoring applications.

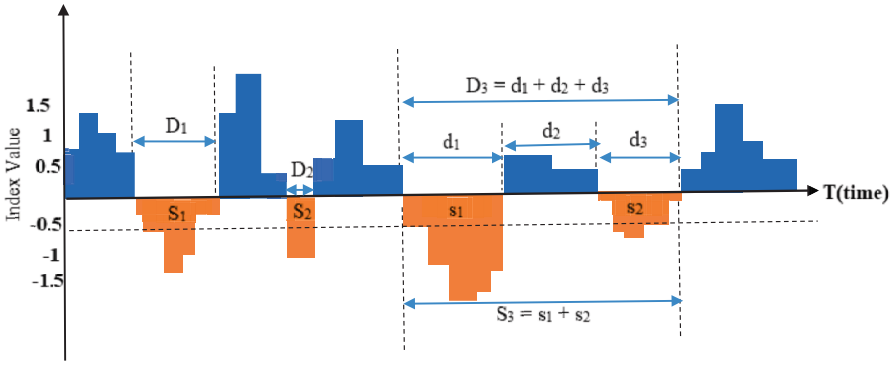

Fig. 3. The run theory-based schematic map for identifying drought characteristics. as duration (D_1, D_2, and D_3), severity (S_1, S_2, and S_3) and intensity ($I_1 = S_1/D_1$, $I_2 = S_2/D_2$ and $I_3 = S_3/D_3$) using the threshold run theory for a given threshold R (Xu et al., 2023). Here R = -0.5.

Table 5
Documented Historical Drought events in the Limpopo and Volta River Basin.

River Basin	Events Period	References
Limpopo River Basin	1982–1983	(Trambauer et al., 2014)
	1991–1992	(GWSA, 2016)
	2002–2003	(Trambauer et al., 2014)
	2015–2016	(GWSA, 2016)
Volta River Basin	1983–1984	(Ndehedehe et al., 2017)
	1997–1998	(Ndehedehe et al., 2017)
	2002–2003	(Ndehedehe et al., 2017)
	2006–2007	(Ndehedehe et al., 2017)

GWPSA: Global Water Partnership Southern Africa.

3. Results

3.1. Optimal distribution functions for drought index calculation

The selection of appropriate probability distributions is critical for accurate drought index calculation. Our analysis of the six candidate distribution functions, evaluated using the Kolmogorov-Smirnov statistic (D), revealed distinct optimal distributions for runoff and soil moisture across different continents (Table 6).

For runoff data, the Log-normal distribution provided the optimal fit in five of six continents (Africa, Asia, Australia, Europe, and North America), with KS statistic values ranging from 0.04 to 0.12. South America was the exception, where the Gamma distribution (D = 0.09) performed best. This continental pattern highlights the predominant right-skewed nature of global runoff distributions, consistent with hydrological processes that typically exhibit positive skewness.

Soil moisture distributions showed greater variability in optimal fitting functions across continents. The Log-normal distribution provided the best fit for Africa and North America (D = 0.16 and 0.18, respectively), while the Normal distribution was optimal for Asia and South America (D = 0.06 and 0.14). The Logistic distribution best characterized soil moisture in Australia and Europe (D = 0.12 and 0.14). This variability reflects the complex interactions between climate regimes, vegetation, and soil characteristics that influence soil moisture dynamics globally.

The optimal distribution functions identified here were subsequently used to calculate the standardized drought indices (SPI, SRI, and SSI) that form the foundation of the CoDI framework. This continent-specific approach to distribution selection enhances the robustness of drought index calculation across diverse hydroclimatic regimes.

3.2. Correlation analysis between CoDI and standard drought indices

To evaluate the integrative capacity of CoDI, we examined its correlation with established drought indices (SPI, SRI, SSI, SPEI_cru, SPEI_era5, scPDSI, and TWSa) at global and basin scales across multiple timescales.

The global correlation patterns between CoDI and other drought indices revealed substantial spatial variability (Fig. 4 and Fig. S1). Fig. 4 illustrates the correlation between CoDI with scPDSI and SPEI-ERA5, which exhibit strong correlations in many regions (Fig. 4a – d). The correlation coefficients often surpass 0.7 in regions including the majority of North America, Australia, southern Africa, most parts of Asia, and northeastern Brazil. In addition, we evaluated the response of Terrestrial Water Storage anomalies (TWSa) derived from the GRAiCE reconstruction product (GRAiCE_BiLSTMnoLCSIF) to CoDI. Fig. 4e and f exhibit the relationship between CoDI and TWSa. We observed strong correlations between the CoDI and TWSa, especially in regions like Australia, central North America, southern South America, South Africa, and certain regions of Asia. The strong correlation between CoDI and TWSa in arid and semi arid regions such central Australia, South Africa, Sahel, some parts of North America, and southern South America during the Pre-GRACE (1984–2001) and during GRACE period (2002–2018), validates CoDI's capacity to accurately depict hydrological deficits.

The maximum global correlation between CoDI and SPEI_cru reached 0.54, 0.98, and 0.68 at 3-, 6-, and 12-month timescales, respectively as shown in Fig. S1. The correlation generally increased with longer timescales across most regions, reflecting the enhanced signal-to-noise ratio at extended temporal aggregations. However, some regions exhibited the opposite pattern, with decreasing correlations at longer timescales, highlighting the complex propagation dynamics of drought across different hydroclimatic systems (You et al., 2025; Zhou et al., 2024).

At the basin scale, correlation analysis revealed strong relationships between CoDI and individual drought indices, with distinct patterns across different river basins (Fig. 5). Despite the length of the study period, the CoDI keeps moderate and strong correlations with SPEI_cru, SPEI_era5, scPDSI, and TWSa. Fig. 5 illustrates the basin-average correlations between CoDI, scPDSI, SPEI-cru, SPEI-era5, and TWSa. A high correlation (dark blue) between CoDI and both SPEI-cru and SPEI-era5 is observed in almost all basins (e.g., Mississippi, Colorado, Zambezi, Ob, Amur, Murray, Sao Francisco), with correlation coefficients (r) surpassing 0.8 (Fig. 5b and c). The Correlation between CoDI and scPDSI exhibit similar pattern (Fig. 5a). This pattern highlights the dominant influence of precipitation and soil moisture anomalies in characterizing drought conditions across these diverse basins.

Moderate correlations (pale blue) with TWSa are observed in several basins including the Ob (ID = 5), Mississippi (ID = 4), Congo (ID = 2), Amazon (ID = 1), and Rio La Plata (ID = 43). Conversely, negative correlations (pale red) were identified in the Mackenzie (ID = 12), Godavari (ID = 54), Ganges (ID = 22), and Brahmaputra (ID = 39) river basins.

The Strong correlations between CoDI and TWSa in some basins (Orange basin, Lake Eyre, Murray, Amur, Uruguay, and Rio Grande)

Table 6
Goodness-of-fit Results for the six distribution functions and parameters of the Runoff and soil moisture in the six continents.

Continents	Distribution	Runoff			Soil Moisture		
		Par 1	Par 2	Ks (D)	Par 1	Par 2	Ks (D)
	Log-Normal	−1.99	1.66	**0.10**	−1.55	0.39	**0.16**
	Gamma	0.52	1.11	0.13	6.38	27.82	0.17
	Weibull	0.63	0.32	0.11	2.53	0.26	0.18
Africa	Exponential	2.15		0.29	4.36		0.45
	Normal	0.46	0.76	0.28	0.23	0.10	0.18
	Logistic	0.31	0.33	0.28	0.22	0.06	0.20
	Log-Normal	−2.61	1.50	**0.11**	−1.32	0.32	0.07
	Gamma	0.39	1.00	0.27	10.24	36.40	0.07
	Weibull	0.54	0.17	0.19	3.11	0.31	0.09
Asia	Exponential	2.5		0.47	3.55		0.40
	Normal	0.39	1.16	0.40	0.28	0.09	**0.06**
	Logistic	0.15	0.32	0.39	0.28	0.05	0.07
	Log-Normal	−2.66	1.59	**0.12**	−1.47	0.24	0.13
	Gamma	0.46	1.65	0.17	16.55	69.94	0.14
	Weibull	0.59	0.16	0.18	3.90	0.26	0.15
Australia	Exponential	3.56		0.35	4.23		0.49
	Normal	0.28	0.59	0.32	0.24	0.06	0.16
	Logistic	0.15	0.21	0.34	0.23	0.04	**0.12**
	Log-Normal	−0.87	1.14	**0.04**	−0.91	0.19	0.20
	Gamma	0.93	1.19	0.12	63.29	0.21	0.21
	Weibull	0.91	0.74	0.10	3.54	0.45	0.29
Europe	Exponential	1.27		0.13	2.43		0.48
	Normal	0.79	1.01	0.25	0.41	0.09	0.25
	Logistic	0.58	0.44	0.22	0.41	0.04	**0.14**
	Log-Normal	−0.25	1.65	0.13	−1.12	0.29	0.16
	Gamma	0.71	0.39	**0.09**	12.70	37.56	0.15
	Weibull	0.82	1.65	0.10	3.76	0.37	0.16
South-America	Exponential	0.55		0.14	2.96		0.38
	Normal	1.82	1.74	0.15	0.34	0.09	**0.14**
	Logistic	1.65	1.00	0.16	0.35	0.05	0.15
	Log-Normal	−2.13	1.47	**0.10**	−0.93	0.50	**0.18**
	Gamma	0.49	1.11	0.17	3.69	8.16	0.22
	Weibull	0.61	0.26	0.14	1.83	0.51	0.25
North-America	Exponential	2.28		0.34	2.21		0.32
	Normal	0.44	1.12	0.35	0.45	0.27	0.29
	Logistic	0.23	0.33	0.34	0.40	0.14	0.19

P1 and P2 are the parameters and ks (D) is the goodness of fit. The bold values are the best fit.

show that CoDI captures the hydrological deficit of these basins by including soil moisture (SSI) and runoff (SRI) components. This is a crucial finding because it validates CoDI as a statistical metric and a physically significant measure of extensive water depletion, which makes it very useful for water resource management applications. Lower correlations in some areas, particularly in basins like Mackenzie, Godavari, Ganges, and Brahmaputra, highlight a known problem for all drought indices and indicate a scope of improvement in the future.

Seasonal correlation analysis further revealed the temporal consistency of CoDI. Across all seasons (Fig. S2), CoDI maintained strong correlations with individual drought indices, demonstrating its robustness for year-round drought monitoring.

The seasonal correlation between CoDI and scPDSI, SPEI-cru, SRI, SSI, and SPI demonstrates a consistent pattern throughout all seasons. Notably, the correlation between CoDI and SRI stands out as the strongest across all seasons and regions, as illustrated in Fig. S2. Nonetheless, we noted a negative correlation in the Sahara and certain regions of Asia between CoDI and SPEI-cru/SSI. A moderate and weak correlation were observed between CoDI and scPDSI in regions such as Central Africa, parts of South America, northern North America, and certain areas of Asia across all seasons. The notably strong correlation between CoDI and SRI in many regions of the Northern Hemisphere during March-April-May, December-January-February, and September-October-November highlights the significance of snowmelt contributions to streamflow during these seasons.

The seasonal correlation coefficient results (Fig. S2) between CoDI and individual drought indices across seasons confirm that CoDI effectively captures the multidimensional nature of drought, integrating meteorological, agricultural, and hydrological drought signals into a unified framework. We observed similar patterns for the seasonal correlations at basin scale as shown in Fig. S3. The CoDI exhibited strong correlation with scPDSI, TWSa, and both SPEI variants.

Moreover, the CoDI demonstrates strong correlations with other indices during the historical drought occurrence in the Danube (ID = 30), Amur (ID = 10), Parana (ID = 6), and Mississippi (ID = 4) river basins, as illustrated in Fig. S4. The CoDI exhibited a strong correlation with TWSa in the Amur basin, a moderate correlation in the Parana and Mississippi basins, and a weak correlation in the Danube basin, with correlation values of 0.73, 0.51, 0.46, and 0.23, respectively. It is noteworthy that all indices had a weak correlation with the TWSa in the Danube basin, indicating the presence of an alternative factor influencing TWSa other than drought. It might be anthropogenic activities like irrigation.

In addition, the time series comparison between CoDI and scPDSI, SPEI_era5, SPEI_cru and TWSa during these historical drought events (Fig. S4) reveals high temporal agreement between the indices, despite some differences in absolute values. scPDSI values were generally more extreme than CoDI, potentially overestimating drought severity in some cases. The more conservative drought severity estimates provided by CoDI suggest it may be less prone to false alarms, an important consideration for operational drought monitoring systems.

Besides, we analyzed the TWSa response to drought conditions as identified by CoDI, scPDSI, SPEI-cru, and SPEI-era5, as illustrated in Fig. 6. The TWSa response to CoDI exhibits a comparable pattern to the two variants of SPEI, with similar short lags (0 to 2 months) in the majority of the 60 selected basins, in contrast to the scPDSI, which displays longer lag times, as illustrated in Fig. 6. The CoDI similarly showed a prolonged lag time of 12 months in the Mackenzie basin with

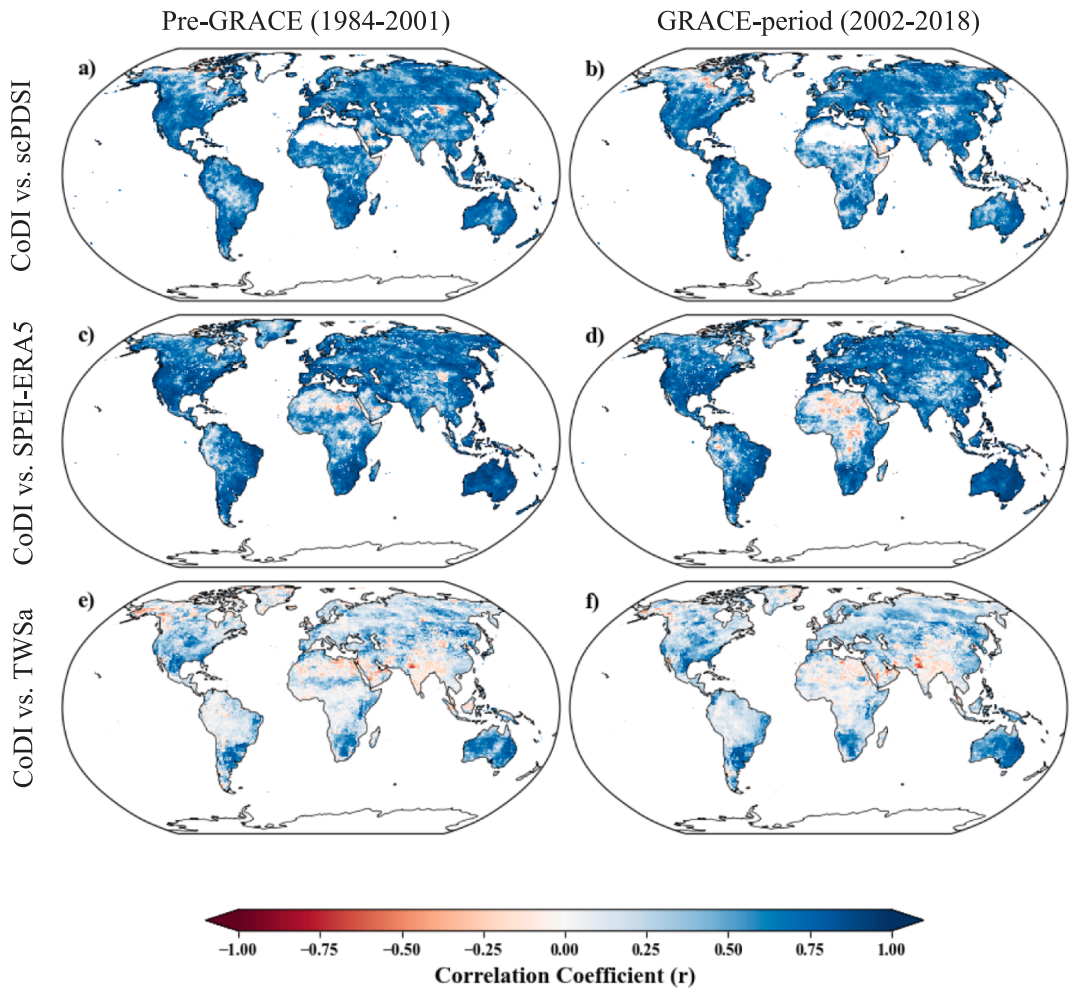

Fig. 4. Correlation coefficient (r) between the codi with spei_era5, twsa, and scpdsi at 12-month timescale during the pre-grace (1984–2001) and during GRACE period (2002–2018) using the reconstructed terrestrial water storage anomaly GRAiCE product (GRAiCE_BiLSTMnoLCSIF). All scenarios are significant at 99% confidence level, and the p-value was approximately equal to zero ($p < 0.05$).

the scPDSI. This finding demonstrates CoDI's capacity to capture the effects of drought and indicates that CoDI is a suitable tool for assessing the impacts of hydrological systems in both the short and long term in response to climatic influences.

3.3. Comparison of drought area detection

The practical utility of any drought index lies in its ability to accurately identify drought-affected areas. We compared the percentage of drought areas (DAP %) detected by CoDI, SPEI-era5, scPDSI, and SPEI_cru across different drought severity classes and timescales for the 60 selected major basins. Fig. 7 illustrates the comparative percentages of extreme drought (ED) areas identified by scPDSI, SPEI-cru, SPEI_era5, and CoDI at a 12-month timescale from 1982 to 2018. The CoDI identified its highest DAP percentages in Nelson (ID = 19), Indus (ID = 27), Orinoco (ID = 25), Sao Francisco (ID = 38), Dnieper (ID = 40), Don (ID = 42), Rio De La Plata (ID = 43), and Shatt Al Arab (ID = 26), with values 8.482, 8.249, 8.129, 8.266, 8.227, 8.238, 8.154, and 8.064, respectively. With lowest DAP % in Godavari (ID = 54), Volta (ID = 46), and Limpopo (ID = 47) with values approximately 2.583, 4.291, and 4.640 respectively.

The CoDI identified a plausible DAP % of extreme drought compared to the scPDSI, which seems to overestimate the intensity of drought occurrences. The sensitivity of scPDSI to temperature may enhance the signal in some locations. The CoDI demonstrates a comparable pattern to the SPEI-era5 over multiple basins in North America and Asia. Nonetheless, the CoDI identified a higher percentage of Extreme drought in the river basins of Africa, Australia, and Europe, as illustrated in Fig. 7c. In addition, the CoDI identified a higher percentage of Extreme Drought in the nine basins of North America compared to the SPEI-cru. A comparable pattern is seen in the basins of southern South America and Europe, as illustrated in Fig. 7b. This reflects the importance of the integration of the CoDI components, including precipitation, runoff, and soil moisture. The SPEI_cru failed to identify areas of extreme drought, whereas the CoDI successfully captured these extreme events. This outcome validates that the CoDI offers a dependable and thorough evaluation of Extreme Drought at the basin scale.

3.4. Seasonal drought detection performance

The ability to accurately identify seasonal drought events is crucial for agricultural planning and water resource management. Fig. 8 shows the seasonal time series of CoDI, SPI, SSI, SRI, and SPEI_cru at the 3-month timescale for the Volta River Basin, with highlighted periods indicating documented seasonal drought events.

All indices successfully captured the major seasonal drought events in the Volta Basin, with CoDI showing patterns consistent with the individual indices. This demonstrates the capacity of CoDI to effectively synthesize drought information from multiple sources while maintaining sensitivity to seasonal drought dynamics.

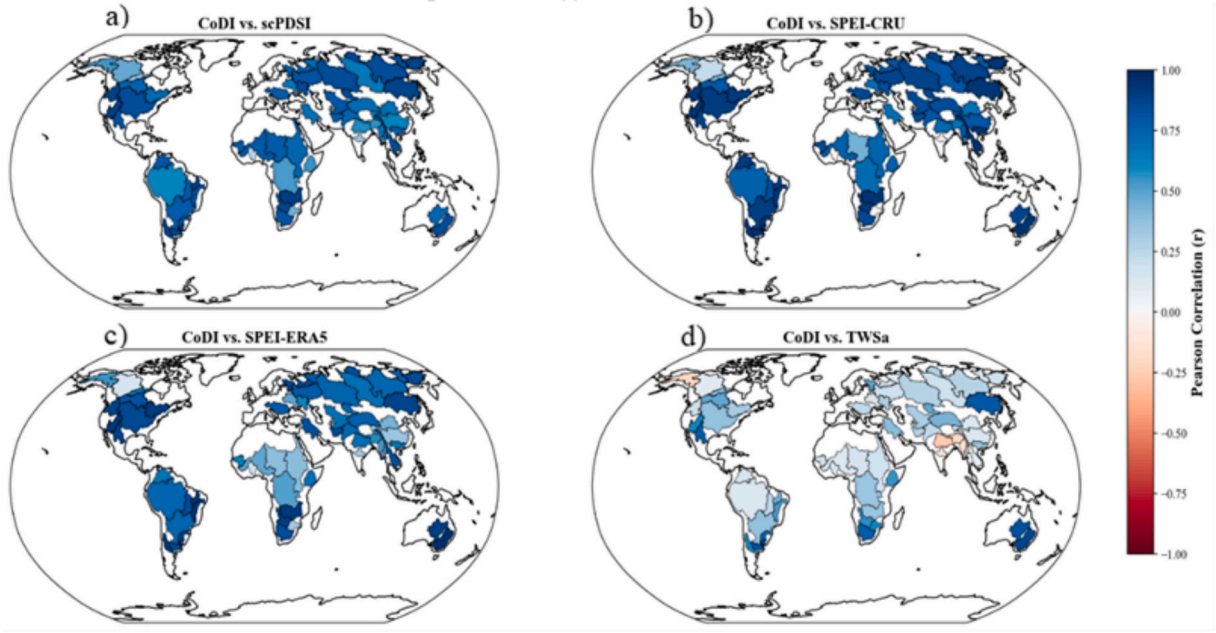

Fig. 5. Correlation coefficient (r) between the codi with a) scpdsi, b) spei-cru, and c) spei_era5 at 12-month timescale from 1982 to 2018 and d) twsa from 1984 to 2018 for the 60 selected river basins. all scenarios are significant at 99% confidence level, and the p-value was approximately equal to zero ($p < 0.05$).

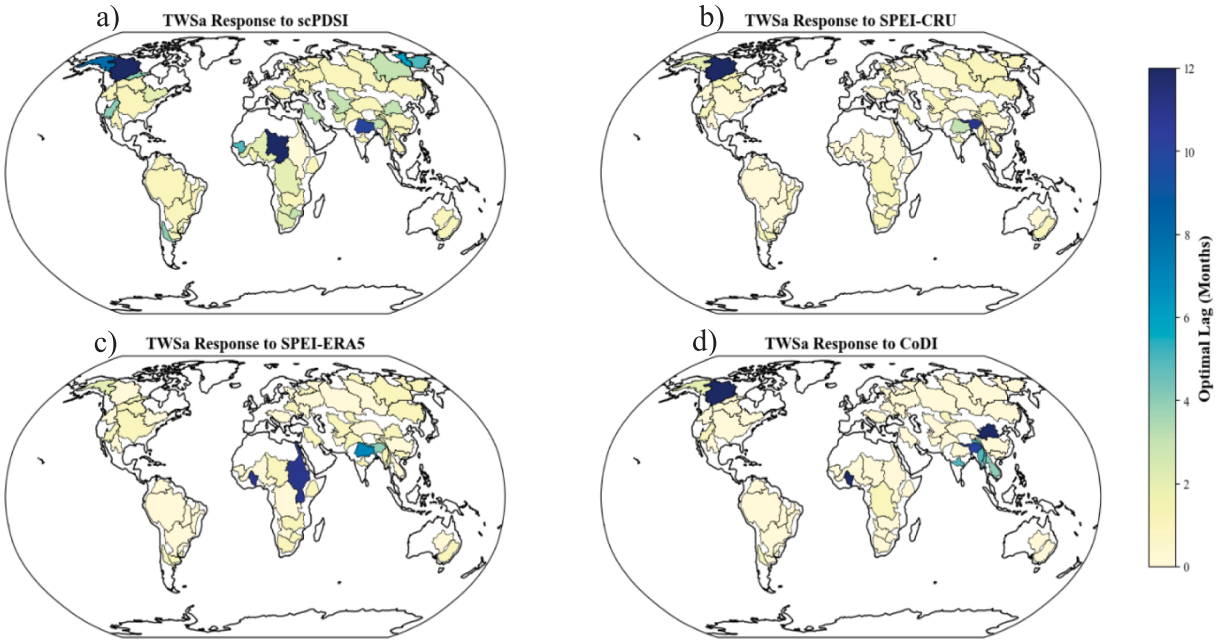

Fig. 6. Comparison of Optimal Lag Time of TWSa response to: a) scPDSI, b) SPEI-cru, c) SPEI-era5, and d) CoDI at 12-month timescale over 1984 to 2018 for the 60 selected river basins.

3.5. Global drought characteristics (1982–2018)

The application of run theory to the global CoDI dataset enabled comprehensive characterization of drought conditions worldwide during the 1982–2018 period. Fig. 9 presents the global spatial distribution of three key drought characteristics: duration, severity, and frequency.

Fig. 9a depicts the Drought duration, which ranged from 40 to 131 months across most regions globally, with the Sahel region, Central Asia, Eastern Brazil, and Central Australia experiencing the longest drought durations. Notably, drought duration patterns did not strictly follow climate zone boundaries, with significant durations observed in both arid and humid regions.

Drought severity showed distinct spatial patterns as we can see from Fig. 9b, with northeastern China, southeastern Russia, the Sahel, Central Africa, Central Asia, northern North America, and parts of South America experiencing the most severe drought conditions. These "drought hotspots" identify regions particularly vulnerable to extreme drought impacts.

Besides, Drought frequency varied considerably across the globe as shown in Fig. 9c, with blue-colored and dark green-colored regions experiencing more frequent drought events than light blue-colored areas.

Moreover, the annual variability of CoDI, SPEI-era5, scPDSI, and SPEI-cru across the 60 river basins reveals distinct temporal patterns of

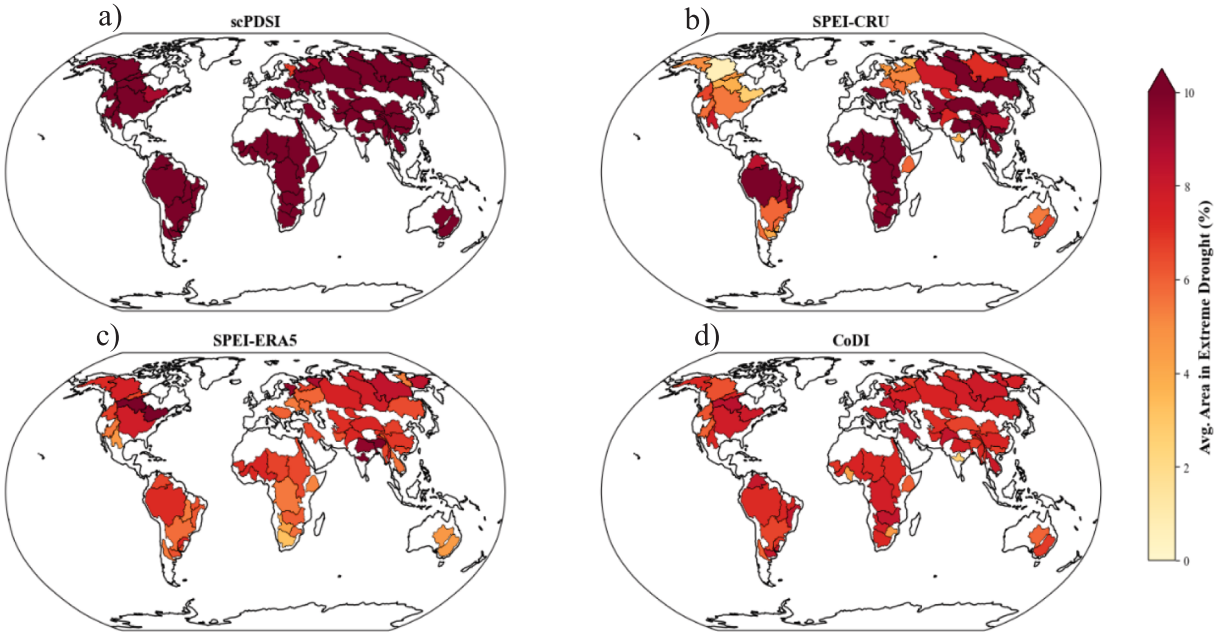

Fig. 7. Comparison of the percentages of drought areas of Extreme Drought (ED) identified by: a) scPDSI, b) SPEI-cru, c) SPEI_era5 and d) CoDI at 12-month timescale over 1982 to 2018 for the 60 selected river basins.

drought occurrence and severity as we can see from Fig. 10. The CoDI exhibit similar patterns to the SPEI variants over multiple basins. The CoDI exhibited its maximum standard deviation in arid and semi-arid river basins, including the Murray, Orange, Eastern Brazil, Columbia, Colorado, and Rio Grande, as illustrated in Fig. 10a. In these regions, slight deviations from average precipitation can result in significant and swift changes in water variability. The CoDI has a standard deviation between 0.2 and 0.9, in contrast to the scPDSI, which displays a distinct pattern compared to the other indices in most of the studied basins (Fig. 10b).

3.6. Validation against historical drought events

The ultimate test of any drought index is its ability to accurately capture documented historical drought events. We validated CoDI against eight well-documented drought events in the Limpopo and Volta River Basins, calculating percentage agreement, RMSE, and correlation coefficient between CoDI and established indices. Table 7 and Table S1 present the results of the aforementioned metrics.

CoDI showed strong correlations with other indices across all historical events, with correlation coefficients ranging from 0.24 to 0.96 (Table 7). From Table 7 we can see that the percentage agreement between CoDI and other indices was generally high, ranging from 20.83% to 95.83%, with corresponding RMSE values (0.226 to 1.350). The highest agreement was observed between CoDI and SRI for the 2006–2007 drought event in the Volta Basin (95.83%, RMSE = 0.308), while the lowest agreement was between CoDI and SSI for the 2015–2016 drought in the Limpopo Basin (20.83%, RMSE = 1.350). In addition, CoDI exhibited a strong correlation with SPEI_cru, SPEI_era5, SPI_era5, and scPDSI in most of the events with a maximum correlation of 0.96 (Table S1).

Fig. 11 and Fig. S5 show the time series comparison between CoDI and other indices for historical drought events in the Volta and Limpopo Basins, respectively. CoDI successfully captured the onset, duration, and termination of these documented drought events, demonstrating consistent patterns with the individual indices. This confirms the ability of CoDI to effectively synthesize drought information from multiple sources while maintaining sensitivity to the temporal dynamics of drought events.

In addition, from Fig. 11, we can see that the CoDI accurately detected these events, including the onset, duration, and termination of all the eight events. Similarly, from Fig. S5, the CoDI shows similar pattern with SPEI_cru, scPDSI, SPEI_era5, and SPI_era5 with approximately the same lag time. This demonstrates the robustness of the integration of meteorological, hydrological, and agricultural components. scPDSI appears to overestimate the severity of these events compare to other indices as shown in Fig. S5.

We have conducted additional analysis to evaluate the performance of the CoDI during these historical events in the Volta and Limpopo basins. We have compared the response of Terrestrial Water Storage to the CoDI, scPDSI, and both variants of SPEI during these events. Fig. 12 and S6 exhibit the comparison of TWSa responses to CoDI, SPEI-cru, SPEI-era5, and scPDSI during these historical drought events.

The CoDI shows a strong correlation with the TWSa across the majority of the historical events in Volta and Limpopo basins compare to the scPDSI. Despite the extreme signal detected by the scPDSI, it presents the lowest correlation with the TWSa among the indices, thereby confirming our assertion that this index overestimates the severity of drought conditions. The CoDI demonstrates comparable patterns with both SPEI variants and exhibits the highest correlation with TWSa, with correlation values of 0.86 and 0.45 during the drought events of 1983 to 1984 and 2002 to 2003 in the Volta basins, respectively, and 0.86 and 0.60 during the drought events of 1991 to 1992 and 2015 to 2016, respectively, in the Limpopo basin. This confirms that the CoDI detected these events and is a useful tool for drought impact assessment.

For regional and continental validation, we compared CoDI with SPEI_cru, SPEI_era5, scPDSI, and SPI_era5 for 14 historical drought events across different regions (Table 8). CoDI showed strong correlations with SPEI_cru and scPDSI across all events, with correlation coefficients ranging from 0.28 to 0.82. The percentage agreement between CoDI and SPEI_cru was consistently high, ranging from 57.36% to 89.76%, with corresponding RMSE values between 0.52 and 1.35. However, the CoDI presents weak correlations with SPEI_era5 and SPI_era5 in detecting some drought events. For instance, the correlation between CoDI and SPEI_era5 for the April 2015 drought event in Niger is 0.08 and the correlation between CoDI and SPI_era5 for the February 2011 drought event in Australia is 0.07. Note that the CoDI had a strong correlation with SPEI_cru and scPDSI during these events. Which

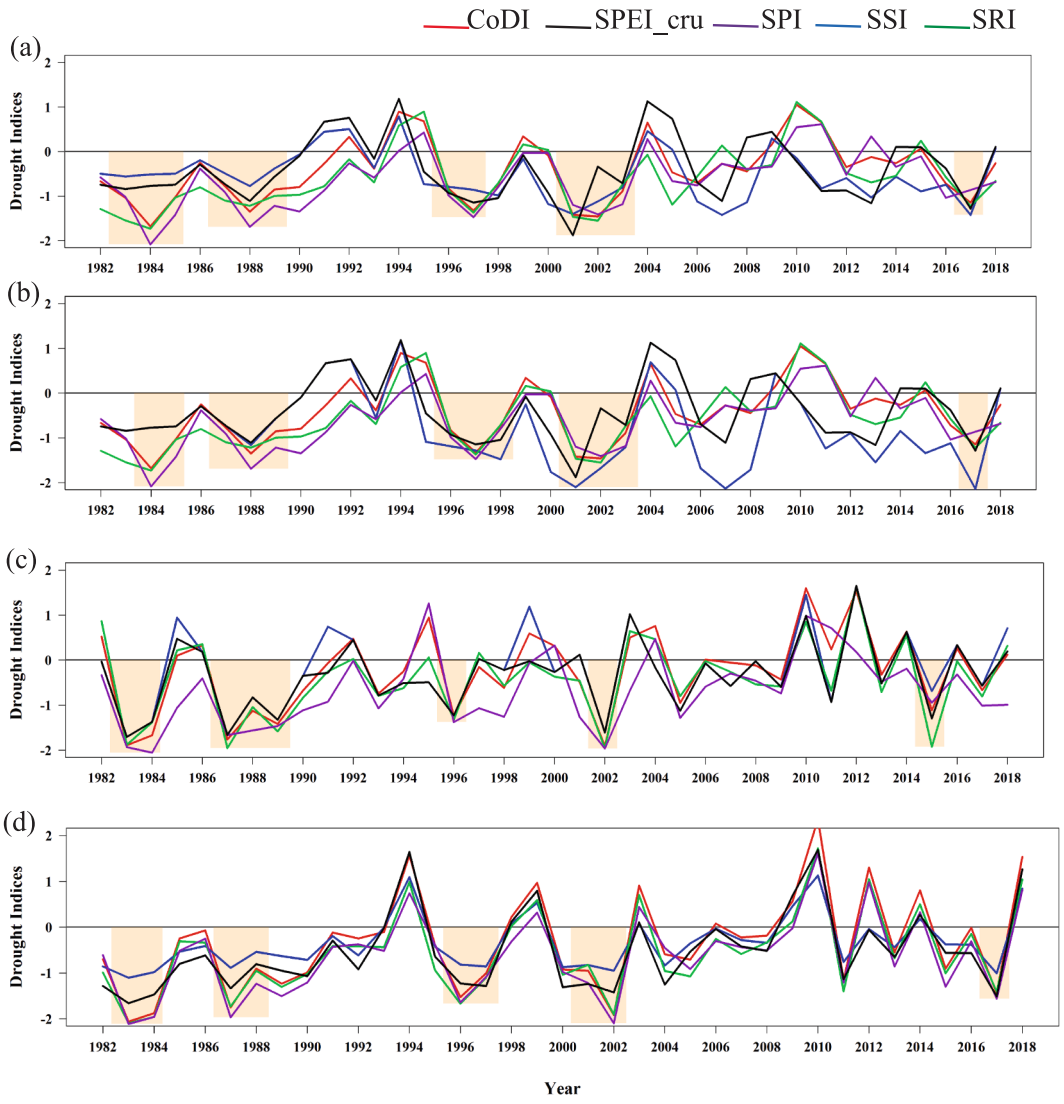

Fig. 8. CoDI, SPI, SRI, SSI, and SPEI_cru time series at the 3-month time scale for the Volta River Basin (VRB) over 1982–2018 in different seasons. The highlights indicate historical seasonal events occurring in this River Basin. (a) Winter, (b) Spring, (c) Summer, and (d) Autumn.

highlight the importance of a comprehensive drought index like the CoDI.

Fig. 13 illustrates the spatial patterns of drought conditions detected by CoDI and SPEI_cru during specific historical events. For the Australian drought events of January-March 2011, CoDI successfully captured all three months of drought conditions, while SPEI_cru only detected the January event. Similarly, CoDI captured the August 2011 drought event in Central Europe, which SPEI_cru failed to detect. These results highlight the enhanced sensitivity of CoDI in identifying specific drought events compared to SPEI_cru.

The comprehensive validation against historical drought events at local, regional, and continental scales confirms the robustness and reliability of CoDI for drought monitoring and characterization across diverse hydroclimatic conditions.

4. Discussion

The development and validation of the CoDI represents a significant advancement in global drought monitoring capabilities. Our findings demonstrate that CoDI effectively integrates meteorological, agricultural, and hydrological drought dimensions into a unified framework that performs consistently across diverse hydroclimatic regimes. Here, we discuss the implications of our results, compare CoDI with existing drought indices, address methodological considerations, and explore potential applications for global drought management.

4.1. Multidimensional drought characterization

CoDI successfully captures the propagation of drought through the hydrological cycle by integrating precipitation anomalies (SPI), soil moisture deficits (SSI), and runoff shortages (SRI). This multidimensional approach represents a key advancement over single-variable indices that cannot reflect the complex cascade of drought impacts across environmental systems (Hao et al., 2016; Yang et al., 2018). The strong correlations between CoDI and established indices at global scale and across diverse basins (Figs. 4 and 5) confirm its ability to synthesize drought information from multiple sources while maintaining sensitivity to the specific drought characteristics of different regions.

Unlike previous composite indices that have primarily focused on regional applications (Han et al., 2022; Jiaoa et al., 2019), CoDI demonstrates robust performance at global, continental, regional, and local scales. Our validation against historical drought events across Africa, Asia, Europe, Australia, and North America (Tables 7 and 8) confirms the global transferability of the CoDI framework. This represents a significant advance over regionally-calibrated indices such as the Composite Multivariate Drought Index (CMDI) for China (Yang et al., 2023),

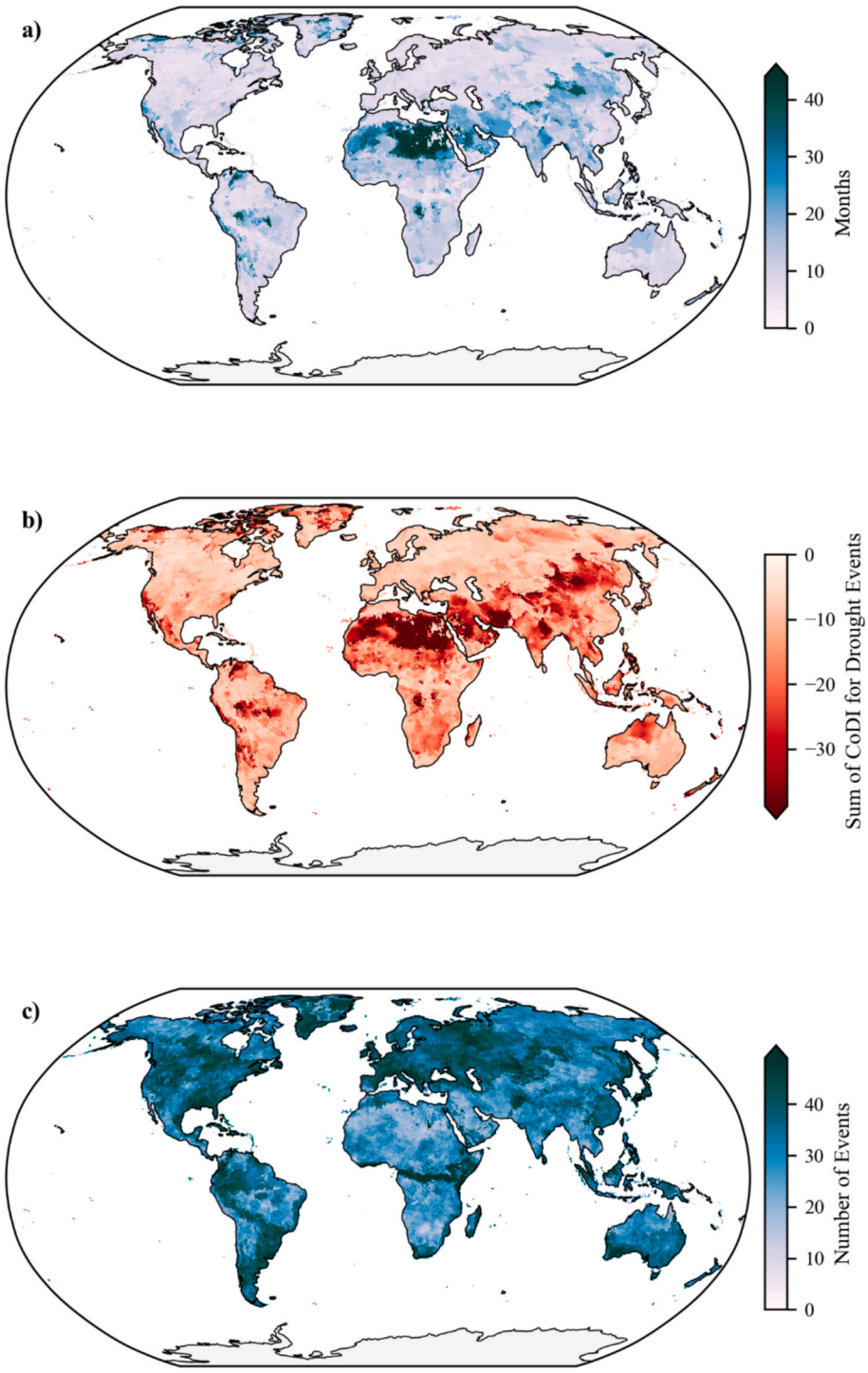

Fig. 9. Spatial Distribution of global drought characteristics detected by the CoDI including (a) Duration, (b) Severity, and (c) Frequency from 1982 to 2018.

the Agricultural Drought Index (agCDI) for Sri Lanka (Bayissa et al., 2022), or the Multivariate Drought Index for the Blue Nile Basin (Ali et al., 2022).

In addition, the global drought characteristics derived from CoDI (Fig. 9) reveal important spatial patterns that transcend traditional climate zone boundaries. For example, our findings show substantial drought durations in both arid regions (e.g., the Sahel and Central Asia) and more humid areas (parts of Southeast Asia and Amazonia). This challenges the conventional assumption that drought frequency and severity are inherently linked to aridity (Chiang et al., 2021). Instead, our results suggest that drought vulnerability depends on complex interactions between atmospheric forcing, land surface conditions, and hydrological processes that vary considerably across space and time.

The identification of global "drought hotspots" with particularly severe or frequent drought conditions (Fig. 9b and c) provides valuable information for prioritizing adaptation measures and developing targeted resilience strategies. Regions such as northeastern China, southeastern Russia, the Sahel, and parts of South America emerged as particularly drought-prone areas during our study period (1982–2018), aligning with independent assessments of global drought vulnerability (Chiang et al., 2021; Ismail et al., 2024).

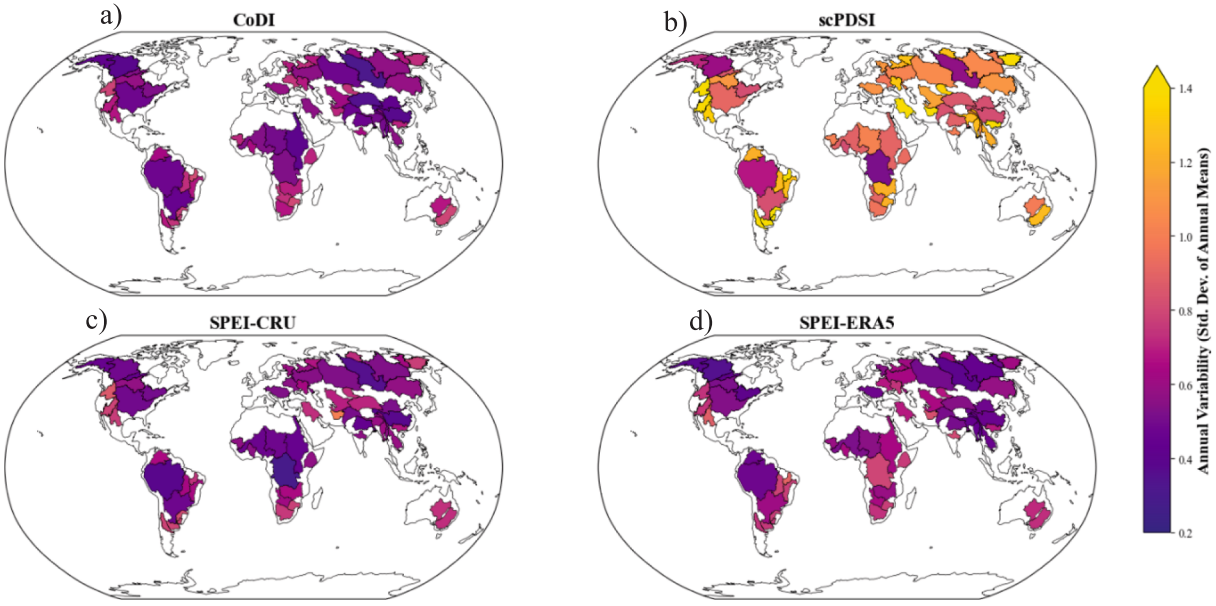

Fig. 10. Annual Variability of: a) CoDI, b) scPDSI, c) SPEI-cru, and d) SPEI-era5 at 12-month timescale over 1982–2018 for the 60 selected River Basin.

Table 7
Percentage of agreement, RMSE, and the correlation between the CoDI with the SPI, SRI, and SSI in capturing the documented historical drought events in the Limpopo and Volta River Basins at the three-month timescale.

River Basin	Events Period	Indices	Agreement (%)	RMSE	Correlation
Limpopo	1982–1983	SPI	87.5	0.514	0.86
		SRI	87.5	0.363	0.94
		SSI	70.83	0.827	0.39
	1991–1992	SPI	87.5	0.558	0.92
		SRI	91.67	0.455	0.92
		SSI	75.00	1.09	0.55
	2002–2003	SPI	91.67	0.304	0.94
		SRI	87.5	0.487	0.95
		SSI	83.33	0.942	0.29
	2015–2016	SPI	75.00	0.528	0.85
		SRI	83.33	0.226	0.91
		SSI	20.83	1.350	0.24
Volta	1983–1984	SPI	95.83	0.402	0.80
		SRI	87.5	0.320	0.82
		SSI	70.83	0.554	0.77
	1997–1998	SPI	54.17	0.694	0.62
		SRI	79.17	0.308	0.93
		SSI	79.17	0.582	0.84
	2002–2003	SPI	91.67	0.562	0.92
		SRI	87.5	0.334	0.96
		SSI	87.5	0.516	0.89
	2006–2007	SPI	87.5	0.535	0.71
		SRI	95.83	0.308	0.85
		SSI	58.33	0.892	0.76

4.2. Drought detection performance

Our comparative analysis of drought area detection by CoDI and other indices (Fig. 7) reveals important differences in how these indices characterize drought severity. CoDI consistently identified moderate average percentage areas of Extreme drought conditions, while scPDSI typically detected more extensive extreme drought areas. This pattern suggests that CoDI may provide more conservative estimates of extreme drought conditions, potentially reducing false alarms in operational drought monitoring systems a critical consideration for drought management decisions that involve significant resource allocations.

In addition, the strong agreement between CoDI and other indices in capturing documented historical drought events (Tables 7 and 8) demonstrates its reliability for operational drought monitoring. Particularly notable is the enhanced sensitivity of CoDI in detecting specific drought events that SPEI_cru failed to capture, such as the Australian drought events of February-March 2011 and the Central European drought of August 2011 (Fig. 13). This improved detection capability is likely attributable to the inclusion of soil moisture and runoff components in CoDI, which capture drought impacts that may not be fully reflected in precipitation and evapotranspiration anomalies alone.

Furthermore, the ability of CoDI to accurately identify drought onset, persistence, and termination (Fig. 11) addresses a critical challenge in drought monitoring systems. Early detection of drought onset enables proactive management responses, while accurate identification of drought termination prevents unnecessary continuation of emergency measures. By integrating information across the meteorological-agricultural-hydrological drought continuum, CoDI provides a more comprehensive representation of drought dynamics than single-variable indices or less integrated composite approaches.

4.3. Methodological innovations and limitations

The continent-specific approach to probability distribution selection represents a methodological innovation that enhances the accuracy of drought index calculation across diverse hydroclimatic regimes. Our analysis revealed distinct optimal distributions for different continents and variables (Table 6), challenging the common practice of applying a single distribution function globally. However, this approach may mask sub-continental variability in statistical distributions, potentially limiting accuracy in regions with highly heterogeneous hydroclimatic conditions. Future refinements could implement more localized distribution selection protocols, perhaps at the scale of major climate zones or hydrological regions.

The Principal Component Analysis framework employed for CoDI construction provides an objective, data-driven method for integrating multiple drought dimensions. By extracting the principal modes of variability from SPI, SSI, and SRI, this approach preserves maximum information content while reducing redundancy. The consistent strong performance of CoDI across diverse validation tests confirms the effectiveness of this integration methodology. However, the fixed weighting of principal components may not optimally capture the relative importance of different drought dimensions in all regions and seasons. Adaptive weighting schemes that account for regional and seasonal variations in drought propagation dynamics could further enhance CoDI

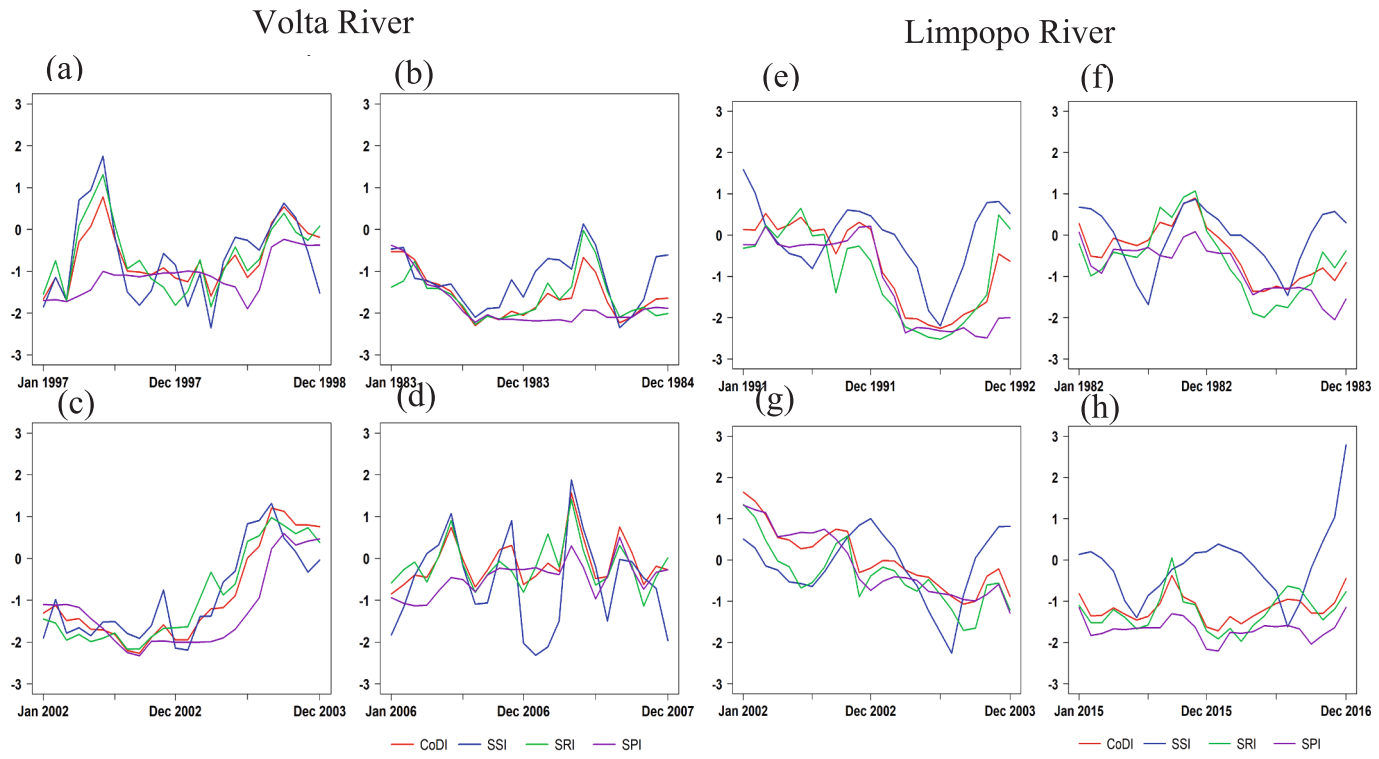

Fig. 11. CoDI, SPI, SRI, and SSI time series for the documented historical drought events in the Volta River Basin a) 1997–1998, b) 1983–1984, c) 2002–2003, and d) 2006–2007 and in the Limpopo River Basin e) 1991–1992, f) 1982–1983, g) 2002–2003, and h) 2015–2016 at the three-month time scale in the Volta River Basin.

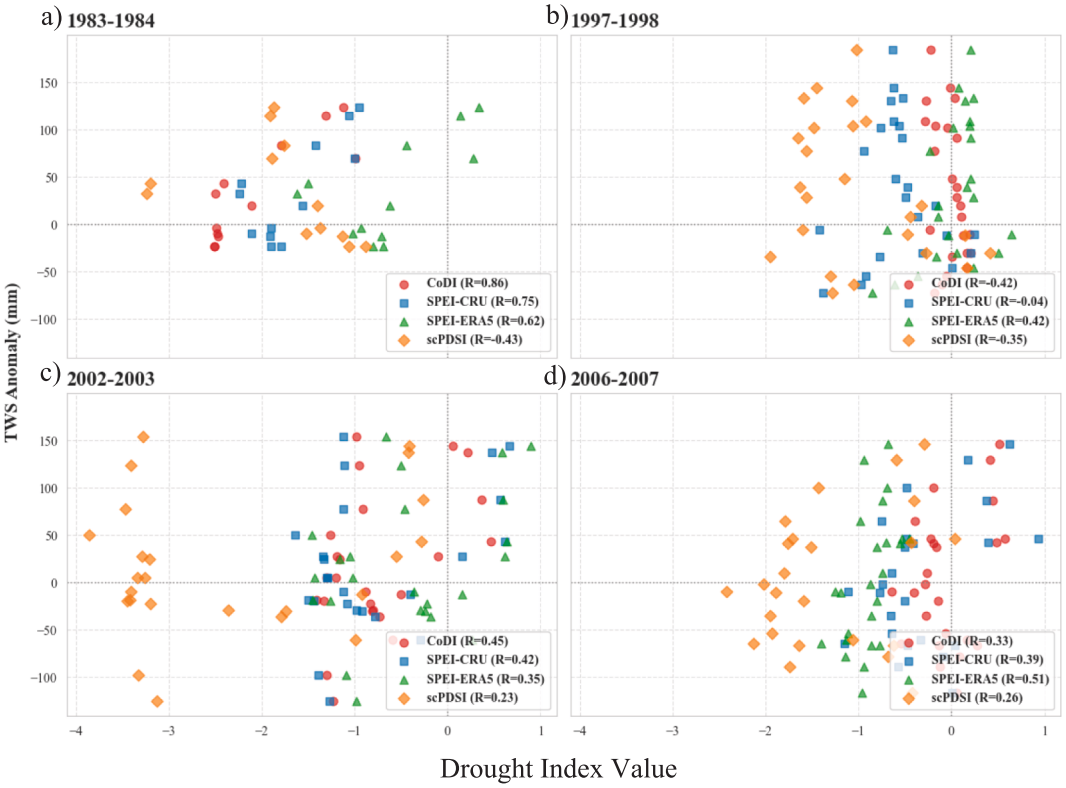

Fig. 12. Comparison of TWSa response to CoDI, SPEI-cru, SPEI-era5, and scPDSI during the historical drought events in the Volta River Basin: a) 1983–1984 (only for the year 1984), b) 1997–1998, c) 2002–2003, and d) 2006–2007.

Table 8
Percentage of agreement, RMSE, and correlation between the CoDI with the SPEI_cru/SPEI_era5/SPI_era5/scPDSI in capturing the documented historical drought events in some regions and continents around the world.

Zone	Event Period	% agreement				RMSE				Correlation			
		SPEI1	SPEI2	SPI	scPDSI	SPEI1	SPEI2	SPI	scPDSI	SPEI1	SPEI2	SPI	scPDSI
Niger	April 2015	71.95	49.83	64.83	37.55	0.96	1.37	1.22	1.25	0.48	0.08	0.32	0.66
Australia	October 2010	89.52	88.54	86.08	88.04	0.73	1.15	1,15	1.09	0.81	0.64	0.52	0.73
Australia	November 2010	89.76	90.13	90.97	87.80	0.76	0.99	1.0	1.20	0.76	0.66	0.59	0.71
Australia	December 2010	88.60	89.90	86.81	88.00	0.80	0.81	1.03	1.29	0.63	0.58	0.46	0.64
Australia	January 2011	59.86	77.29	73.48	86.30	1.19	1.07	1.22	1.39	0.40	0.20	0.11	0.54
Australia	February 2011	66.15	90.62	88.09	87.80	0.96	0.93	0.97	1.41	0.49	0.01	0.07	0.58
Australia	March 2011	70.44	89.79	88.19	86.03	0.82	1.01	1.00	1.61	0.58	0.31	0.31	0.50
China	April 2013	67.13	69.44	63.84	72.79	1.18	1.03	1.12	1.63	0.70	0.64	0.46	0.60
EE + SR + K	July 2010	79.29	80.74	75.42	76.23	0.78	0.80	0.96	1.84	0.82	0.79	0.67	0.62
EE	August 2010	83.60	80.62	76.14	77.31	1.02	1.01	1.06	1.88	0.77	0.67	0.57	0.64
EE	September 2010	74.63	70.44	67.80	72.19	1.25	1.20	1.28	2.08	0.58	0.40	0.31	0.48
EE	October 2010	57.36	52.40	52.72	65.64	1.35	1.34	1.16	2.12	0.47	0.29	0.24	0.40
Sahel	August 2011	84.59	76.81	64.52	78.31	0.52	0.96	1.22	1.29	0.71	0.04	−0.07	0.45
Sahel	April 2012	69.03	81.86	71.13	70.78	0.85	0.89	0.86	1.10	0.55	0.24	0.47	0.28

Note: EE = Eastern Europe, SR = Southwestern Russia, K = Kazakhstan, SPEI1=SPEI_cru, SPEI2=SPEI_era5, SPI=SPI_era5.

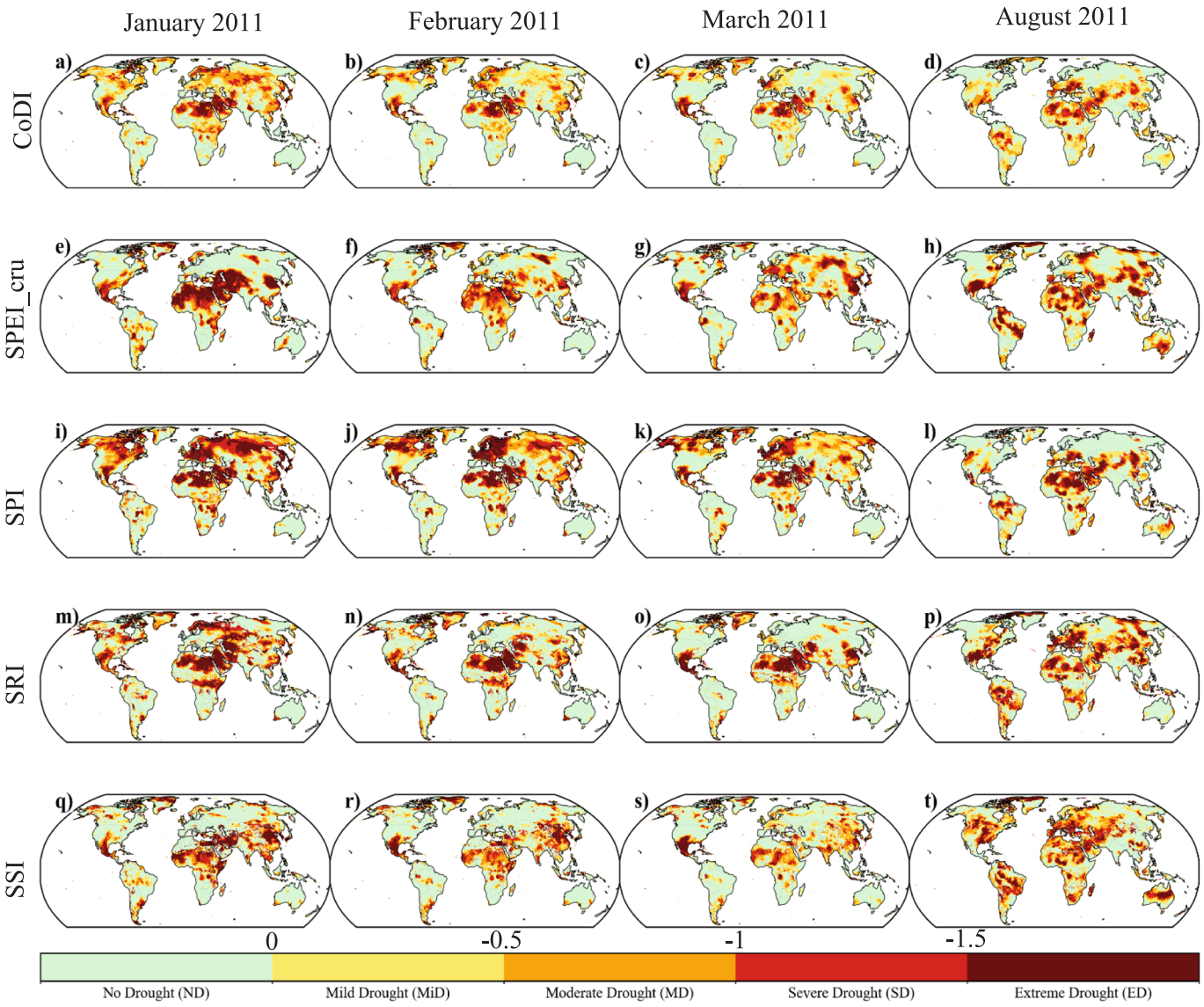

Fig. 13. Spatial distribution of drought conditions monitored by CoDI, SPEI_cru, SPI, SRI, and SSI for the year 2011.

performance.

The global datasets used in this study provide consistent, long-term coverage necessary for robust drought characterization. However, these reanalysis and model-derived products inevitably contain uncertainties and biases that propagate through the CoDI framework. Particularly in regions with sparse observational networks (e.g., parts of Africa and Central Asia), these uncertainties may reduce the reliability of drought assessments. Integration of emerging remote sensing products, particularly from missions with enhanced soil moisture and evapotranspiration retrieval capabilities, could improve the accuracy of CoDI in data-sparse regions.

4.4. Applications for drought management and climate adaptation

The multi-scalar nature of CoDI, with calculations at 3-, 6-, and 12-month timescales, enables targeted applications across sectors with different drought response characteristics. The 3-month CoDI effectively captures meteorological drought conditions relevant for agricultural planning and early warning systems. The 6-month timescale corresponds well with seasonal agricultural drought impacts, while the 12-month CoDI better represents hydrological drought conditions affecting water resource systems and long-term planning (Fig. S7).

CoDI provides a valuable tool for monitoring drought under changing climate conditions. The annual variability analysis (Fig. 10) reveals increasing drought fluctuations in several basins in recent decades, consistent with climate change projections of intensifying hydrological extremes (Chiang et al., 2021; Fabian et al., 2023). By providing consistent, multidimensional drought characterization, CoDI can support assessment of drought trends and attribution studies linking drought patterns to climate forcing.

The global approach of CoDI enables consistent cross-regional drought comparison and monitoring a critical capability for international water management, transboundary water negotiations, and global food security assessments. The framework can be readily implemented in operational drought monitoring systems and early warning platforms, providing decision-makers with comprehensive information on developing drought conditions across multiple dimensions of the hydrological cycle. The framework can be utilized by many stakeholders, including water resource managers and river basin authorities, who may employ the index for early warning systems and water allocation. Agricultural planners can utilize this measure to estimate the demand for irrigation and alleviate potential crop yield reductions during prolonged droughts.

Beyond operational monitoring, CoDI offers valuable capabilities for validating climate model projections of future drought conditions. The consistent global framework enables direct comparison with climate model outputs, facilitating improved assessment of projected changes in drought characteristics under different climate scenarios. This application has significant implications for adaptation planning, infrastructure design, and long-term water resource management under climate change.

4.5. Future research directions

While CoDI represents a significant advancement in global drought monitoring, several promising research directions could further enhance its capabilities. Integration of additional drought-related variables, such as vegetation condition indices, groundwater anomalies, and snow water equivalent could provide even more comprehensive drought characterization, particularly for specific ecosystems or hydrological regimes where these components play critical roles. Developing regionally and seasonally adaptive weighting mechanisms for index integration would better reflect the varying importance of different drought dimensions across space and time, potentially improving performance in regions with distinct drought propagation dynamics. Expanding the framework to examine interactions between drought and other extremes (e.g., heatwaves, wildfires) would address the growing challenge of compound climate hazards, enabling more holistic risk assessment and management strategies. Targeted validation efforts in regions with limited observational networks would increase confidence in CoDI performance globally, especially in data-sparse areas where current drought monitoring is particularly challenging. Finally, adapting the methodology for operational, near-real-time drought monitoring would maximize its utility for early warning systems and adaptive management, bridging the gap between research advances and practical drought response capabilities.

The robust performance of CoDI across diverse hydroclimatic regimes and validation tests demonstrates its potential as a comprehensive tool for global drought monitoring and characterization. By integrating meteorological, agricultural, and hydrological drought perspectives, CoDI provides a more holistic representation of drought conditions than previously possible, with critical applications for water resource management, agricultural planning, disaster risk reduction, and climate adaptation strategies. This framework represents an important step toward transforming drought management from reactive to proactive approaches through improved detection, consistent characterization, and enhanced understanding of drought dynamics across the global hydrological cycle.

5. Conclusion

The CoDI presented in this study represents a significant advancement in global drought monitoring capabilities by effectively integrating meteorological, agricultural, and hydrological dimensions of drought into a unified framework. Through rigorous testing and validation across diverse hydroclimatic regions, we have demonstrated that CoDI provides reliable, consistent drought characterization at multiple spatial and temporal scales.

Our findings reveal several key innovations in drought monitoring methodology: (1) the optimal integration of precipitation, soil moisture, and runoff anomalies through Principal Component Analysis preserves maximum information content while reducing redundancy; (2) the continent-specific approach to probability distribution selection enhances accuracy across diverse climate regimes; and (3) the multi-scalar implementation enables targeted applications across sectors with different drought response characteristics.

Global drought analysis using CoDI identified important spatial patterns in drought duration, severity, and frequency during the 1982–2018 period. Regions including the Sahel, Central Asia, northeastern China, and parts of South America emerged as particular drought hotspots, while the comprehensive validation against historical drought events confirmed CoDI's enhanced sensitivity in detecting drought onset, persistence, and termination compared to established indices.

The practical applications of CoDI extend across multiple domains: early warning systems benefit from its improved drought detection capabilities; water resource managers gain comprehensive insights into hydrological drought dynamics; agricultural planning can leverage the agricultural drought dimension; and climate adaptation strategies can utilize consistent drought characterization for vulnerability assessment and resilience planning.

As climate change intensifies hydrological extremes globally, the need for robust, integrative drought monitoring approaches becomes increasingly critical. CoDI provides a powerful framework for understanding drought complexity across the Earth system, supporting the transformation from reactive to proactive drought management strategies. Future refinements incorporating additional drought-related variables, dynamic weighting schemes, and operational implementation could further enhance this approach, ultimately strengthening global capacity for drought resilience in a changing climate.

CRediT authorship contribution statement

Alhassane Bah: Writing – original draft, Visualization, Validation, Software, Methodology, Investigation, Formal analysis, Data curation, Conceptualization. **Asim Biswas:** Writing – review & editing. **Hao Feng:** Writing – review & editing. **Qiang Yu:** Writing – review & editing. **Qianfeng Wang:** Writing – review & editing. **Yi Li:** Validation, Supervision, Resources, Project administration, Funding acquisition.

Declaration of competing interest

The authors declare that they have no known competing financial interests or personal relationships that could have appeared to influence the work reported in this paper.

Acknowledgements

This work was supported by the National Natural Science Foundation (No. 52079114 and 52350410451), the Natural Science Foundation of Shenzhen (No. CYJ20220530161403007), and the High-end Foreign Experts Introduction Projects (No. s 20240082, H20240401 and S20240161).

Appendix A. Supplementary data

Supplementary data to this article can be found online at https://doi.org/10.1016/j.jhydrol.2026.135413.

Data availability

Data will be made available on request.

References

Ali, M., Ghaith, M., Wagdy, A., Helmi, A.M., 2022. Development of a new multivariate composite drought index for the blue nile river basin. Water (Switzerland) 14 (6), 1–24. https://doi.org/10.3390/w14060886.

Balint, Z., Mutua, F., Muchiri, P., Omuto, C.T., 2013. *Monitoring drought with the combined drought index in kenya*. Developments in Earth Surface Processes 16, 341–356. https://doi.org/10.1016/B978-0-444-59559-1.00023-2.

Bayissa, Y., Srinivasan, R., Joseph, G., Bahuguna, A., Shrestha, A., Ayling, S., Punyawardena, R., Nandalal, K.D.W., 2022. Developing a combined drought index to monitor agricultural drought in Sri Lanka. Water (switzerland) 14 (20), 3317. https://doi.org/10.3390/w14203317.

Beck, H.E., Zimmermann, N.E., McVicar, T.R., Vergopolan, N., Berg, A., Wood, E.F., 2018. Present and future köppen-geiger climate classification maps at 1-km resolution. Sci. Data 5, 1–12. https://doi.org/10.1038/sdata.2018.214.

Cai, S., Zuo, D., Wang, H., Xu, Z., Wang, G., Yang, H., 2023. Assessment of agricultural drought based on multi-source remote sensing data in a major grain producing area of Northwest China. Agric Water Manag 278, 108142. https://doi.org/10.1016/j.agwat.2023.108142.

Chiang, F., Mazdiyasni, O., AghaKouchak, A., 2021. Evidence of anthropogenic impacts on global drought frequency, duration, and intensity. Nat. Commun. 12 (1), 1–10. https://doi.org/10.1038/s41467-021-22314-w.

Ndehedehe, C.E., Awange, J.L., Kuhn, M., Nathan, O., Agutu, Y.f., 2017. *Analysis of hydrological variability over the Volta river basin using in-situ data and satellite observations*. J. Hydrol.: Reg. Stud. 12, 88–110. https://doi.org/10.1016/j.ejrh.2017.04.005.

Dilanka Athukoralalage, A.J.B., McDowell, R.W., Mosley, L.M., 2021. Impact of hydrological drought occurrence, duration, and severity on Murray-Darling basin water quality. Water Res. 252, 121201. https://doi.org/10.1016/j.watres.2024.121201.

Du, L., Tian, Q., Yu, T., Meng, Q., Jancso, T., Udvardy, P., Huang, Y., 2013. A comprehensive drought monitoring method integrating MODIS and TRMM data. Int. J. Appl. Earth Obs. Geoinf. 23 (1), 245–253. https://doi.org/10.1016/j.jag.2012.09.010.

Fabian, P.S., Kwon, H.H., Vithanage, M., Lee, J.H., 2023. Modeling, challenges, and strategies for understanding impacts of climate extremes (droughts and floods) on water quality in Asia: a review. Environ. Res. 225, 115617. https://doi.org/10.1016/j.envres.2023.115617.

Ghiggi, G., Humphrey, V., Seneviratne, S.I., Gudmundsson, L., 2019. GRUN: an observation-based global gridded runoff dataset from 1902 to 2014. Earth Syst. Sci. Data 11 (4), 1655–1674. https://doi.org/10.5194/essd-11-1655-2019.

GWSA. 2016. Limpopo river basin disaster preparedness action plan (Final draft): Enhancing resilience to water-related disaster risks. Limpopo Water Course Commission (LIMCOM).https://limpopocommission.org/download/limpopo-basin-disaster-risk-reduction-strategy-and-action-plan/.

Han, J., Zhang, J., Yang, S., Cao, D., Ahmed Prodhan, F., Pangali Sharma, T.P., 2022. A new composite index for global soil plant atmosphere continuum drought monitoring combing remote-sensing based terrestrial water storage and vapor pressure deficit anomalies. J. Hydrol. 615 (PA), 128622. https://doi.org/10.1016/j.jhydrol.2022.128622.

Hao, Z., AghaKouchak, A., 2013. Multivariate standardized drought index: a parametric multi-index model. Adv. Water Resour. 57, 12–18. https://doi.org/10.1016/j.advwatres.2013.03.009.

Hao, Z., Hao, F., Singh, V.P., 2016. A general framework for multivariate multi-index drought prediction based on Multivariate Ensemble Streamflow Prediction (MESP). J. Hydrol. 539, 1–10. https://doi.org/10.1016/j.jhydrol.2016.04.074.

Herweijer, C., Seager, R., 2008. The global footprint of persistent extra-tropical drought in the instrumental era. Int. J. Climatol. 1774, 1761–1774. https://doi.org/10.1002/joc.

Ian, H., Osborn, T.J., Phil, J., Lis, D., 2020. Version 4 of the CRU TS monthly high-resolution gridded multivariate climate dataset. Sci. Data 7 (1), 1–18. https://doi.org/10.1038/s41597-020-0453-3.

Ismail, M., Li, Y., Niu, B., Ghaffar, M.A., Saleem, M.A., Siddique, K.H.M., 2024. A multi-sensor drought index for improved agricultural drought monitoring and risk assessment in the heterogeneous landscapes of the China–Pakistan Economic Corridor (CPEC). Atmos. Res. 310, 107633. https://doi.org/10.1016/j.atmosres.2024.107633.

Jiefeng, Wu., Liu, Z., Yao, H., Chen, X., Chen, X., Yanhui Zheng, Y.H., 2018. Impacts of reservoir operations on multi-scale correlations between hydrological drought and meteorological drought. J. Hydrol. 563, 726–736. https://doi.org/10.1016/j.jhydrol.2018.06.053.

Johnny Jesudhas, C.C.J.T., Roy, T., 2024. Remote sensing-based drought hazard monitoring and assessment in a coastal plain: a principal component approach. Environ. Res. 243 (2023), 117757. https://doi.org/10.1016/j.envres.2023.117757.

Keune, J., Di Giuseppe, F., Barnard, C., Damasio da Costa, E., Wetterhall, F., 2025. ERA5–Drought: global drought indices based on ECMWF reanalysis. Sci. Data 12 (1), 1–13. https://doi.org/10.1038/s41597-025-04896-y.

Kumar, V., Chu, H.J., 2024. Seasonal drought severity identification using a modified multivariate index: a case study of Indo-Gangetic Plains in India. J. Hydrol. 629, 130632. https://doi.org/10.1016/j.jhydrol.2024.130632.

Leeper, R. D., Petersen, B., Palecki, M. A., & Diamond, and H. 2021. *Exploring the Use of Standardized Soil Moisture as a Drought Indicator*. *2005*, 1021–1033. Doi: 10.1175/JAMC-D-20-0275.1.

Liu, Q., Zhang, S., Zhang, H., Bai, Y., Zhang, J., 2020. Monitoring drought using composite drought indices based on remote sensing. Sci. Total Environ. 711, 134585. https://doi.org/10.1016/j.scitotenv.2019.134585.

Liu, Y., Zhu, Y., Ren, L., Yong, B., Singh, V.P., Yuan, F., Jiang, S., Yang, X., 2019. On the mechanisms of two composite methods for construction of multivariate drought indices. Sci. Total Environ. 647, 981–991. https://doi.org/10.1016/j.scitotenv.2018.07.273.

Mishra, A.K., Singh, V.P., 2010. A review of drought concepts. J. Hydrol. 391 (1), 202–216. https://doi.org/10.1016/j.jhydrol.2010.07.012.

Mukherjee, S., Mishra, A., Trenberth, K.E., 2018. Climate change and drought: a perspective on drought indices. Current Climate Change Reports 4 (2), 145–163. https://doi.org/10.1007/s40641-018-0098-x.

Niu, B., Li, Y., Li Liu, D., Xie, L., Wang, L., Jiang, X., Feng, H., Yu, Q., He, J., Lin, H., 2024. Improved identification and monitoring of meteorological, agricultural, and hydrological droughts using the modified nonstationary drought indices in the Yellow River Basin of China. J. Hydrol. 643, 131788. https://doi.org/10.1016/j.jhydrol.2024.131788.

Palazzoli, I., Ceola, S., Gentine, P., 2025. GRAiCE: reconstructing terrestrial water storage anomalies with recurrent neural networks. Sci. Data 12 (1), 1–13. https://doi.org/10.1038/s41597-025-04403-3.

Pendergrass, A.G., Meehl, G.A., Pulwarty, R., et al., 2020. *Flash droughts present a new challenge for subseasonal-to-seasonal prediction*. Nat. Clim. Chang. 10, 191–199. https://doi.org/10.1038/s41558-020-0709-0.

Rajsekhar, D., Singh, V.P., Mishra, A.K., 2015. Multivariate drought index: an information theory based approach for integrated drought assessment. J. Hydrol. 526, 164–182. https://doi.org/10.1016/j.jhydrol.2014.11.031.

Sabut, A., Mishra, A., 2026. A century of drought research (1900–2023): scientific developments, methodological innovations, and emerging frontiers. Water Resour. Res. 62 (1), e2025WR041987. https://doi.org/10.1029/2025WR041987.

Stagge, J.H., Tallaksen, L.M., Gudmundsson, L., Van Loon, A.F., Stahl, K., 2015. Candidate distributions for climatological drought indices (SPI and SPEI). Int. J. Climatol. 35 (13), 4027–4040. https://doi.org/10.1002/joc.4267.

Trambauer, P., Maskey, S., Werner, M., Pappenberger, F., Van Beek, L.P.H., Uhlenbrook, S., 2014. Identification and simulation of space-time variability of past hydrological drought events in the Limpopo River basin, southern Africa. Hydrol. Earth Syst. Sci. 18 (8), 2925–2942. https://doi.org/10.5194/hess-18-2925-2014.

Van Der Schrier, G., Barichivich, J., Briffa, K.R., Jones, P.D., 2013. A scPDSI-based global data set of dry and wet spells for 1901–2009. J. Geophys. Res. Atmos. 118 (10), 4025–4048. https://doi.org/10.1002/jgrd.50355.

Wang, W., Yang, H., Huang, S., Wang, Z., Liang, Q., Haodan, C., 2024. Trivariate copula functions for constructing a comprehensive atmosphere-land surface-hydrology drought index: a case study in the Yellow River basin. J. Hydrol. 642, 131784. https://doi.org/10.1016/j.jhydrol.2024.131784.

Wells, N., Goddard, S., Hayes, M.J., 2004. A self-calibrating palmer drought severity index. J. Clim. 17 (12), 2335–2351. https://doi.org/10.1175/1520-0442(2004)017<2335:ASPDSI>2.0.CO;2.

Jiaoa, W., Wanga, L., Kimberly, A., Novickb, Q.C., 2019. *A new station-enabled multi-sensor integrated index for drought monitoring*. J. Hydrol. 574, 169–180. https://doi.org/10.1016/j.jhydrol.2019.04.037.

Wu, J., Chen, X., Yao, H., Zhang, D., 2021. Multi-timescale assessment of propagation thresholds from meteorological to hydrological drought. Sci. Total Environ. 765, 144232. https://doi.org/10.1016/j.scitotenv.2020.144232.

Xu, H., Zhu, Y., Levent Yagci, A., Lü, H., Gou, Q., Wang, X., Liu, E., Ding, Z., Pan, Y., Liu, D., Bah, A., 2023. Development of composite drought indices for the coastal areas of southeastern China: a case study of Jinjiang and Jiulongjiang River basins. J. Hydrol. 626 (PA), 130210. https://doi.org/10.1016/j.jhydrol.2023.130210.

Yang, B., Cui, Q., Meng, Y., Zhang, Z., Hong, Z., Hu, F., Li, J., Tao, C., Wang, Z., Zhang, W., 2023. Combined multivariate drought index for drought assessment in China from 2003 to 2020. Agric Water Manag 281, 108241. https://doi.org/10.1016/j.agwat.2023.108241.

Yang, J., Chang, J., Wang, Y., Li, Y., Hu, H., Chen, Y., Huang, Q., Yao, J., 2018. Comprehensive drought characteristics analysis based on a nonlinear multivariate drought index. J. Hydrol. 557, 651–667. https://doi.org/10.1016/j.jhydrol.2017.12.055.

You, Z., Sun, X., Sun, H., Chen, L., Lu, M., Xue, J., Ban, X., Yan, B., Tuo, Y., Qin, H., Zhang, L., Zhang, W., 2025. Mechanisms of meteorological drought propagation to agricultural drought in China: insights from causality chain. Npj Natural Hazards 2, 24. https://doi.org/10.1038/s44304-025-00073-8.

Zhang, G., Ali, S., Wang, X., Wang, G., Pan, Z., Zhang, J., 2019. SPI-based drought simulation and prediction using ARMA-GARCH model. Appl. Math Comput. 355, 96–107. https://doi.org/10.1016/j.amc.2019.02.058.

Zhang, Y., Liu, X., Jiao, W., Zeng, X., Xing, X., Zhang, L., 2021. Drought monitoring based on a new combined remote sensing index across the transitional area between humid and arid regions in China. Atmos. Res. 264, 105850. https://doi.org/10.1016/j.atmosres.2021.105850.

Zhou, Z., Wang, P., Li, L., Fu, Q., Ding, Y., Chen, P., Xue, P., Wang, T., Shi, H., 2024. Recent development on drought propagation: a comprehensive review. J. Hydrol. 645 (PB), 132196. https://doi.org/10.1016/j.jhydrol.2024.132196.